Energy Conversion and Management 351 (2026) 121050

Contents lists available at ScienceDirect

Energy Conversion and Management

journal homepage: www.elsevier.com/locate/enconman

Research Paper

Techno-economic modeling and assessment of a binary power plant for the utilization of two-phase geothermal fluids

Fernando Montesdeoca-Martínez [a,b,*], Sergio Velázquez-Medina [b], Stefan Kranz [c]

[a] Doctoral School, University of Las Palmas de Gran Canaria, Juan de Quesada 30, 35001 Las Palmas de Gran Canaria, Canary Islands, Spain
[b] Group for the Research on Renewable Energy Systems (GRRES), University of Las Palmas de Gran Canaria, Campus de Tafira s/n, 35017 Las Palmas de Gran Canaria, Canary Islands, Spain
[c] GFZ Helmholtz Centre for Geosciences, Telegrafenberg, 14473 Potsdam, Germany

ARTICLE INFO

Keywords:
Geothermal energy
Power plant
Binary cycle
Thermodynamic modelling
Process design
Techno-economic assessment

ABSTRACT

This paper presents an original design of a binary power plant for the utilization of two-phase geothermal fluids from liquid-dominated fields. The proposed plant concept includes an innovative design aspect based on an additional evaporator for the condensation of previously separated geothermal steam. The model of the proposed system is implemented, and a parametric study conducted through simulations to measure the effect of different process and component design variables on thermodynamic performance. Three dry organic fluids, n-pentane, isopentane, and n-butane, were selected for the thermodynamic analysis. A comparative study was also undertaken to determine whether the proposed system could improve upon the specific power output and economic performance of a single-flash system and a flash-binary system under the same geothermal resource conditions. A maximum net power output of 13.59 MW was achieved using n-pentane as the working fluid for a turbine inlet temperature of 175 °C, a wellhead pressure of 13 bar, and an approach temperature difference in the dry cooler of 16 K. The results of the comparative study showed that the proposed system offers both thermodynamic and techno-economic benefits over other geothermal energy systems. Although capital expenditure for the proposed design is 5.6% higher than that for the single-flash system, a more than doubled specific power output ensures a better economic performance. Additionally, the proposed design shows a specific power output improvement of up to 25.6% compared to the flash-binary system while capital expenditure is 19.2% lower.

1. Introduction

Renewable electricity generation is an effective option for mitigating climate change while strengthening pathways to sustainable development [1]. Its deployment is particularly essential on islands which, given their insular and remote nature, tend to be extremely dependent on fossil fuels and have low levels of integration in global energy markets [2]. Consequently, the European Union has launched initiatives to help small island territories produce low-cost sustainable energy in situ and improve their energy security [3]. In this regard, given the high availability of renewable energy sources (RESs) on various islands, numerous studies have been published in the literature concerning their exploitation [4]. Wind and solar photovoltaic (PV) are present in most of the papers examined in a literature review on electricity generation on islands [4]. However, the variable nature of these RESs [5,6] entails an additional difficulty for the energy system to achieve the required balance between the fluctuating energy input and the prevailing demand [7]. If such a balance is not achieved, power system effects may arise such as frequency instability or voltage fluctuations [7], which can be even more detrimental in the case of islands as these usually present weaker electricity grid structures and are more sensitive to power quality issues [8].

Unlike other RESs, geothermal energy can provide consistent baseload power [9]. As it uses natural heat in the ground its operation is practically uninfluenced by surface weather conditions [10], allowing a constant and reliable production of electricity. Additionally, geothermal power plants can provide grid frequency stabilization during a disturbance [11]. In this regard, geothermal energy can reliably replace fossil fuels in the electricity generation structure [12]. Incorporation of this alternative RES can play an important role within the framework of energy sustainability strategies given it significant contribution to reducing greenhouse gas emissions [13]. It should be noted that both its CO_2 emissions [14] and water requirements [10] are low compared to

* Corresponding author.
E-mail address: fernando.montesdeoca@ulpgc.es (F. Montesdeoca-Martínez).

https://doi.org/10.1016/j.enconman.2026.121050
Received 20 August 2025; Received in revised form 3 January 2026; Accepted 5 January 2026
Available online 9 January 2026

Nomenclature

Abbreviations

CAPEX	capital expenditure
CEPCI	Chemical Engineering Plant Cost Index
CI	capital investment
EES	Engineering Equation Solver
EOS	equations of state
GWP	global warming potential
NCG	non-condensable gases
ODP	ozone depletion potential
ORC	organic Rankine cycle
PEC	purchased equipment cost
PI	productivity index
POD	power optimum design
PV	photovoltaic
RES	renewable energy sources
SPO	specific power output
TIT	turbine inlet temperature

Subscripts

0	ambient
a	air
A	additional
ap	approach
C	condenser
CP	cooling water pump
CW	cooling water
D	destruction
DC	dry cooler
E	evaporator
el	electrical
F	fan
G	generator
gf	geothermal fluid
i	inlet
l	liquid
LM	logarithmic mean
m	mixture
mec	mechanical
o	outlet
P	working fluid pump
PH	preheater
pp	pinch point
R	reservoir
REC	recuperator
s	isentropic
S	separator
st	steam
T	turbine
th	thermal
u	utilization
wf	working fluid

Symbols

A	area (m^2)
cp	specific heat (kJ/kg·°C)
d	diameter (m)
$\dot{E}$	exergy rate (kW)
f_m	Moody friction factor for two-phase mixtures (dimensionless)
g	gravity (m/s^2)
h	specific enthalpy (kJ/kg)
$\dot{m}$	mass flow rate (kg/s)
p	pressure (bar)
$\dot{Q}$	heat flow rate (W)
Re	Reynolds number (dimensionless)
s	specific entropy (kJ/kg·K)
T	temperature (°C)
U	overall heat transfer coefficient ($W/m^2 \cdot K$)
$\dot{V}$	volumetric flow rate (m^3/s)
v	velocity (m/s)
$\dot{W}$	power (W)
x	vapor quality (dimensionless)
z	elevation (m)

Greek symbols

Λ	roughness parameter (dimensionless)
ε	roughness (m)
η	efficiency (dimensionless)
μ	viscosity (kg/(m·s))
ϱ	density (kg/m^3)

other energy sources. Likewise, the land occupation requirements are less than for other renewable sources such as wind [10] or solar PV [15].

Of the geothermal technologies that have been proposed for the production of electricity, organic Rankine cycles (ORCs) are notable for their adaptability to a wide resource temperature range [16] and their ability to rapidly ramp production up or down [17]. In addition, as they operate in a closed-loop mode with the direct return of fluids to depth, no liquid or gaseous emissions are generated [18], which means a lower environmental impact compared to other geothermal generation technologies [19]. Currently, binary cycle power plants constitute 14% of geothermal power generation capacity [20], with single-flash, dry steam and double-flash technologies constituting 42%, 23% and 19%, respectively, of the global geothermal capacity [20]. However, the ORC industry is evolving [21], and geothermal energy, together with small waste heat installations, are expected to be among the most important heat sources in the coming years [22].

ORC technology is most commonly used to exploit low- to medium-temperature liquid-dominated geothermal heat sources [22]. Several studies have been published in the literature on the performance of ORC systems for the exploitation of low-grade energy sources. Many of these focus on important technical aspects of binary power plants, such as working fluid selection, process design and component design. He et al. [23] used the maximum net power output, suitable working pressure, total heat transfer capacity and expander size parameter as criteria to screen the working fluids of the ORC. Madhawa Hettiarachchi et al. [24] employed the ratio of the total heat exchanger area to net power output as objective function to compare the optimum cycle performance for different working fluids. Dai et al. [25] examined the effects of turbine inlet pressure and temperature on ORC performance and selected exergy efficiency as the objective function for parameter optimization. Papadopoulos et al. [26] developed a multi-objective computer-aided molecular design method to design working fluids for optimum ORC performance. They identified both novel and conventional working fluids covering a very broad range of potential performance characteristics. Shengjun et al. [27] caried out a parameter optimization and performance comparison of the working fluids in a low-temperature binary geothermal power system. For the optimization procedure they considered five indicators: thermal efficiency, exergy efficiency, recovery efficiency, heat exchanger area per unit power output and the levelized energy cost.

Despite many preceding studies, an optimal power generation system for high-temperature (>150 °C [28]) liquid-dominated reservoirs remains unreported [29]. According to DiPippo [30], geothermal power plants have evolved from relatively simple dry steam systems to complicated multi-flash and hybrid systems designed to operate on liquid-dominated reservoirs. There are hybrid systems in which ORC technology can be integrated or combined with flash cycles. In combined systems, the ORC is used as a bottoming unit for heat recovery of the brine from the topping unit [31]. The performance of such types of complex geothermal systems has been explored in various papers. Abdolalipouradl et al. [32] proposed four novel flash-binary-based cycles (single flash-ORC, two double flash-ORC variations, and triple flash-ORC) for the Sabalan geothermal field (Iran). It was concluded from a comparative analysis that the single flash-ORC with R123 working fluid had the best exergoeconomic performance. Pratama and Koike [29] compared the performance of the single-flash, double-flash, and flash-binary cycles using a high-temperature geothermal fluid at 230–350 °C. In the flash-binary system, the flash cycle unit was combined with an ORC subunit, with the latter fed by the geothermal liquid at 180 °C after the separator. The flash-binary cycle achieved the highest total power (17.6 MW), although the authors noted the caution that needs to be taken about concluding this to be the best system as the reinjection brine temperature was lower than that of the single- and double-flash cycles. Hsieh et al. [33] developed a high-temperature geothermal reservoir model and coupled it with a flash–binary cycle model to investigate the performance and economics of the system. The authors stressed that the first-law efficiency of the ORC was higher than that of the single-flash cycle and was unaffected by the production temperature and flash pressure. It should be noted that, although the impact of flash pressure on the performance and economics of the flash-binary cycle was analyzed, only one working fluid (isobutane) was considered, and values were set for the evaporator temperature and the pinch point temperature difference in the evaporator and condenser. Shokati et al. [34] undertook a comparative study of double-flash and single flash-ORC combined cycles based on exergoeconomic criteria. They highlighted that although the single flash-ORC achieved higher first-law and exergy efficiency values, the double-flash cycle presented the minimum unit cost of produced power. Mokarram and Mosaffa [35] carried out a thermoeconomic analysis of two enhanced flash geothermal cycles integrated with transcritical and subcritical ORCs. They assumed a heat source temperature of 250 °C for the analysis. The results showed that the transcritical ORC increased power production by up to 3.25% in comparison with the subcritical one. However, certain design assumptions had to be made to prevent oscillating properties around the critical point.

A non-standard ORC plant concept developed to exploit high-temperature geothermal resources has been reported in the literature which involves separating geothermal steam and introducing it into the evaporator to evaporate the organic working fluid [36]. The geothermal condensate at evaporator outlet is then mixed with the hot separated brine to provide preheating medium for the organic working fluid. This binary two-phase configuration has been used since 1994 at the Ribeira Grande commercial geothermal power plant (Phase A), located on the island of São Miguel (Azores, Portugal) [36]. Years later, new production wells were drilled to expand the net capacity from 5 to 13 MW (Phase B) [37]. In the same geothermal field, the 10 MW Pico Vermelho plant began operating in 2006. It is based on the same design concept and uses n-pentane as the working fluid. According to Franco et al. [37], each well at the latter plant produces an average of 100–150 t/h of geothermal fluid at 200 °C. The same design concept was used for Unit 1 of the 13 MW Olkaria III geothermal power plant in Kenya, commissioned in 2000 [38]. According to Tranamil-Maripe et al. [39], the same plant concept is used at the Cerro Pabellón geothermal power plant located in Pampa Apacheta (Chile). This plant began operating in 2017, employing two twin binary units, each with a capacity of 24 MW [40]. In these units, the steam stream is introduced into a heat exchanger to evaporate isopentane [39]. The mixture of geothermal condensate and brine is used to preheat the isopentane. Following a recent expansion, the plant now has a total capacity of 81 MW [41]. In this case, the temperature of the geothermal fluid can reach up to 260 °C. Another variant of the steam-condensing binary configuration was analyzed by Jalilinasrabady et al. [42]. In this case, the working fluid (R134a) in the compressed liquid state enters the evaporator directly, where the geothermal steam is condensed. The system model was developed and validated using actual data from a site experiment. Specifically, a mass flow rate of 0.03864 kg/s of separated steam and 0.4346 kg/s of R134a was used to achieve a net power output of 4.19 kW. After conducting an energy and exergy analysis, they highlighted that the working fluid reaches the superheated region without a preheating medium.

The literature review found that the hybridization of different types of geothermal energy conversion systems is a commonly adopted solution for the use of high-temperature geothermal resources extracted from liquid-dominated reservoirs. However, this solution involves design complexity, difficulty in maintenance, and high costs [30]. Solutions based on steam-condensing binary configurations are also found in various scientific publications. However, these consist primarily of demonstrations of the startup and operation of existing commercial plants or small-scale experiments. Furthermore, in most of these proposals, the heat quantities of steam and condensate/brine mixtures are similar to the heat quantities for boiling and preheating the working fluid, respectively. In contrast to ORCs using single-phase geothermal sources, steam-condensing binary configurations still lack broad support in the literature, especially in terms of techno-economic evaluations of the system. This paper aims to propose an innovative design aspect for a non-combined binary power plant configured to optimize the use of a two-phase fluid from a high-temperature geothermal field. The innovation is based on the incorporation of an additional evaporator in which the separated geothermal steam is condensed to partially evaporate the working fluid, while the remainder of its evaporation and preheating are achieved by cooling the condensate/brine mixture in other heat exchangers. A numerical model of the two-phase geofluid and the aboveground system is implemented using a programming software tool. A parametric analysis is developed through simulations in order to identify the effect of different process and component design variables on the thermodynamic performance of the system. The parameters that are varied in the analysis are wellhead pressure, turbine inlet temperature, pinch point temperature difference in the preheater and approach temperature difference in the dry cooler. Three environmentally friendly organic working fluids were selected for the analysis. The analysis employs an optimization approach which includes a search for the specific configuration which maximizes the net plant power output. The thermodynamic and economic performance of the optimal ORC design is then compared with other reference geothermal systems under the same geothermal fluid conditions at the wellhead. Parameters such as the specific power output (SPO), the utilization efficiency and capital expenditure (CAPEX) are compared. The resulting process and component design parameters can serve as a basis for the development of specific geothermal energy integration strategies. The developed method can be used to estimate the maximum net electrical power that can be harnessed by this technology based on the conditions of a specific geothermal reservoir. In this paper, it is applied to a case study on the island of Tenerife (Spain).

2. Method

2.1. System description

The layout of the proposed ORC system for the use of two-phase geothermal fluids is shown in Fig. 1. By opting for binary technology, the geothermal plant has two separate circulating systems in which the geothermal fluid and the working fluid are confined. Since a two-phase flow is expected in the high-temperature geothermal production well

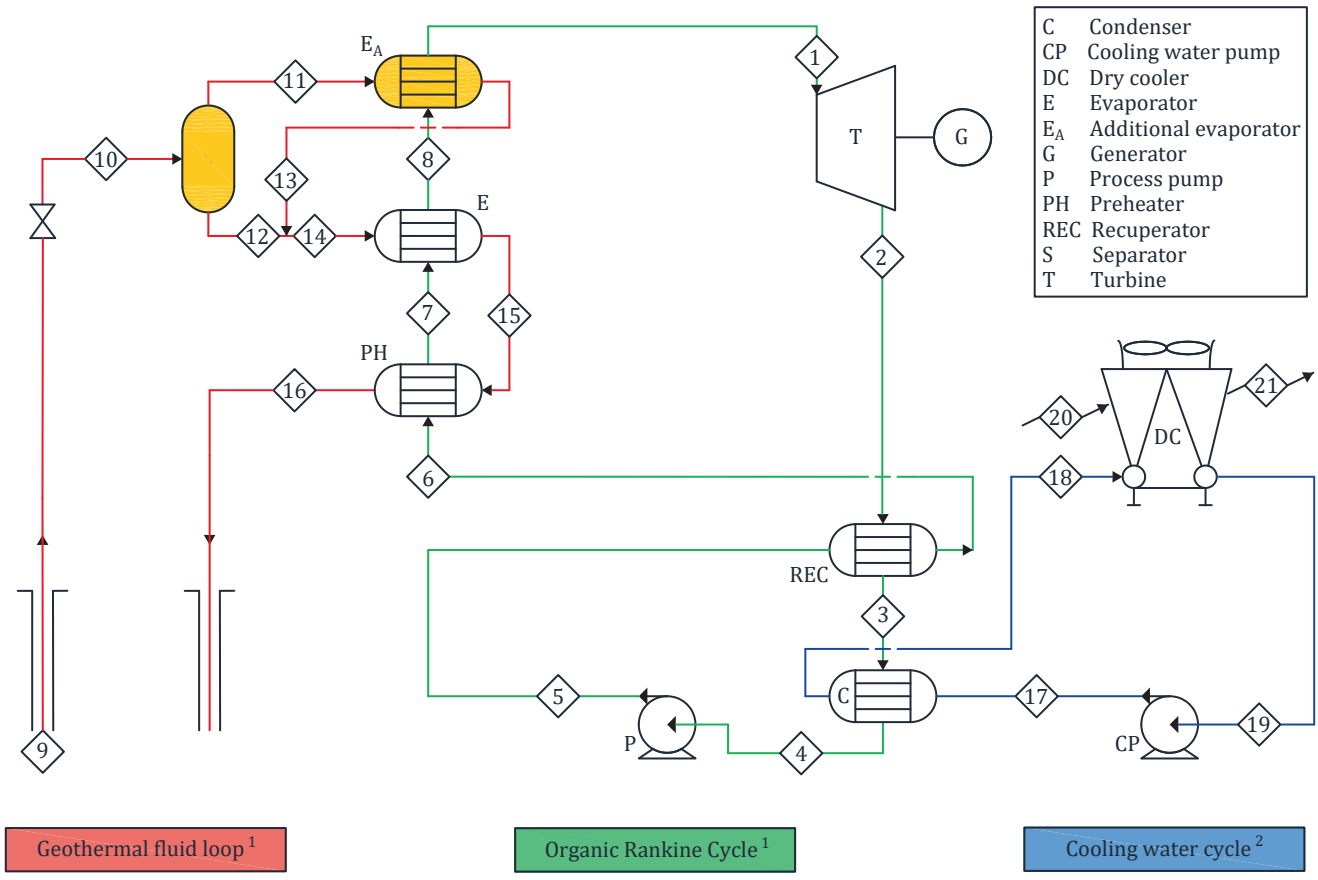

Fig. 1. Layout of the geothermal power plant. Notes: [1] The additional equipment incorporated in the proposed model compared to the traditional recuperative ORC is highlighted in yellow; [2] Heat rejection is performed indirectly through a closed cooling water loop and air-cooled heat exchangers.

[43], a separator is added to which the two-phase fluid stream (stream 10) enters and from which a saturated steam stream (stream 11) and a saturated liquid stream (stream 12) exit. The steam stream 11 is introduced into the evaporator E_A to partially evaporate the working fluid. By transferring heat to the working fluid, the steam condenses in evaporator E_A, resulting in an outlet stream of geothermal condensate in saturated liquid state (stream 13). The brine stream 12 is mixed with the condensate stream 13 to supply the heat required for the remaining partial evaporation and the preheating of the working fluid in evaporator E and the preheater, respectively. After its passage through the preheater, the geothermal brine stream in subcooled liquid state (stream 16) is reinjected into the geothermal reservoir. The non-condensable gases (NCGs) would be removed in the evaporator E_A, then bypass the power plant and be reinjected into the reservoir.

The subcritical ORC is selected as the conversion cycle, given the practical operating difficulties and safety concerns [44] that the supercritical cycle may present, as well as the need for more expensive devices [45]. The ORC unit has the equipment required to subject the working fluid to thermodynamic processes, namely a turbine, a recuperator, a condenser, and a pump, in addition to the preheater and the evaporators E and E_A. The recuperator is included due to its importance in high-temperature applications in terms of improving system efficiency and reducing the heat released to the environment [45]. Regarding heat dissipation, the use of dry coolers was proposed to avoid the use of water. However, it was finally decided to employ indirect heat rejection through a closed cooling water loop for various reasons, most notably the reduction in the condenser volume and the pressure losses of the working fluid at turbine discharge [46]. This loop is equipped with a pump for the circulation of the cooling water.

Fig. 2 shows the temperature-entropy diagram of the subcritical ORC

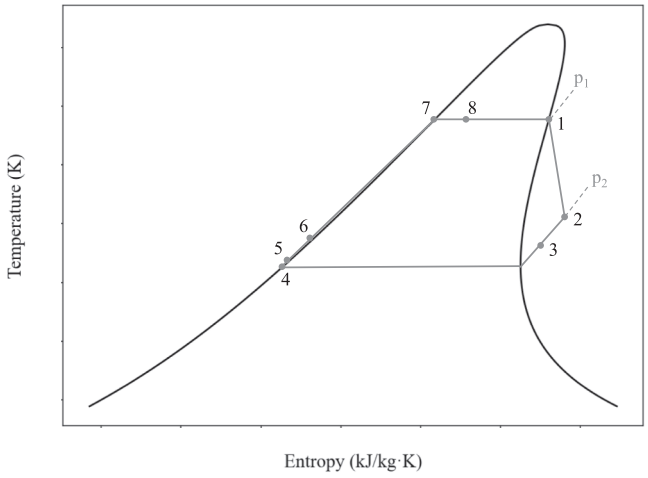

Fig. 2. Temperature-entropy diagram of the subcritical ORC with retrograde fluid.

with retrograde fluid, whose positive slope allows for dry expansion [47]. In thermodynamic state 1, the working fluid enters the turbine in a saturated vapor state and expands to the pressure corresponding to state 2, which is in the superheated region. In the expansion process, the working fluid delivers work to the turbine shaft, which is coupled to an electric generator. The superheated working fluid enters the recuperator to decrease its temperature from T_2 to T_3 before entering the condenser, where it will transfer heat to the cooling water until it reaches the saturated liquid state at state 4. Subsequently, a pump raises the

pressure of the working fluid from p_4 to p_5, with the latter corresponding to the high-level pressure. The pressurized liquid working fluid enters the recuperator to raise its temperature from T_5 to T_6. The heat given off by the geothermal fluid in the preheater is used to increase the temperature of the working fluid to T_7, reaching the saturated liquid state. In evaporator E, the saturated liquid working fluid absorbs heat from the geothermal fluid until it reaches state 8, where it is in liquid–vapor equilibrium. The working fluid enters a second evaporator E_A to reach state 1. Note that the processes of heat recovery, condensation, preheating, and evaporation of the working fluid are treated as near isobaric due to the small pressure drops across the heat exchangers.

2.2. System modelling and simulation

A model of the system was implemented using the programming software Engineering Equation Solver (EES) [48]. The developed code includes the numerical model of the two-phase fluid and the aboveground system. The development of the two-phase fluid modeling was based on fundamental equations of momentum and energy transport. The aboveground system model was fundamentally developed following detailed energy balance equations in the different ORC equipment. To determine the thermophysical properties of the states, the built-in thermophysical property functions of EES were used. A parametric study was conducted to analyze the influence of certain parameters, both operational and design, on system performance.

Fig. 3 shows a schematic representation of the methodology followed to obtain the output parameters.

As can be seen in Fig. 3, a set of general assumptions is employed for system modeling and simulation. The following general assumptions are considered in the present study:

(1) A tubing inside diameter of 22.4 cm and a pipe-roughness factor of $2.5{\cdot}10^{-5}$ m for production wells [49].
(2) A 2% pressure drop of the geofluid and the working fluid in each heat exchanger [50].
(3) An airside pressure drop of 200 Pa in the dry cooler [51].
(4) A temperature difference of 10 °C between the superheated working fluid at the outlet of the recuperator (state 3) and the subcooled liquid working fluid at its inlet (state 5).
(5) A temperature difference of 10 °C between the cooling water at the dry cooler inlet T_{18} and the air at the dry cooler outlet T_{21}.
(6) A liquid temperature difference in the dry cooler of 5 °C [52].
(7) A cooling water pump head of 15 m [53].
(8) Constant specific heats of the cooling water cp_{CW} and air cp_a of 4.186 and 1.005 kJ/kg·K, respectively.
(9) The assumed component efficiencies are shown in Table 1.

The developed method can be generally applied to specific case studies in which the intention is to exploit a two-phase geofluid extracted from a liquid-dominated field by means of the ORC system described in subsection 2.1. As can be seen in Fig. 3, the model requires the introduction by the user of five input parameters with the specific site conditions, namely the reservoir temperature, pressure and depth, the productivity index, and the ambient temperature.

2.2.1. Two-phase fluid modelling

The productivity index (PI) is defined as the flow rate per unit pressure drop (Eq. (1)) [54]. The pressure drop Δp is the difference between the initial static pressure in the reservoir, p_R, and the flowing bottom-hole pressure at the well, p_9 [55].

$$\mathrm{PI} = \frac{\dot{\mathrm{V}}}{\Delta \mathrm{p}} \tag{1}$$

Table 1
Assumed component efficiencies [91,92].

Parameter	Value
Turbine isentropic efficiency ($\eta_{s,T}$)	0.85
Process pump isentropic efficiency ($\eta_{s,P}$)	0.80
Turbine mechanical efficiency ($\eta_{mec,T}$)	0.95
Generator efficiency ($\eta_{el,G}$)	0.95
Process pump efficiency (η_P)	0.70
Cooling water pump efficiency (η_{CP})	0.70
Fan efficiency (η_F)	0.60

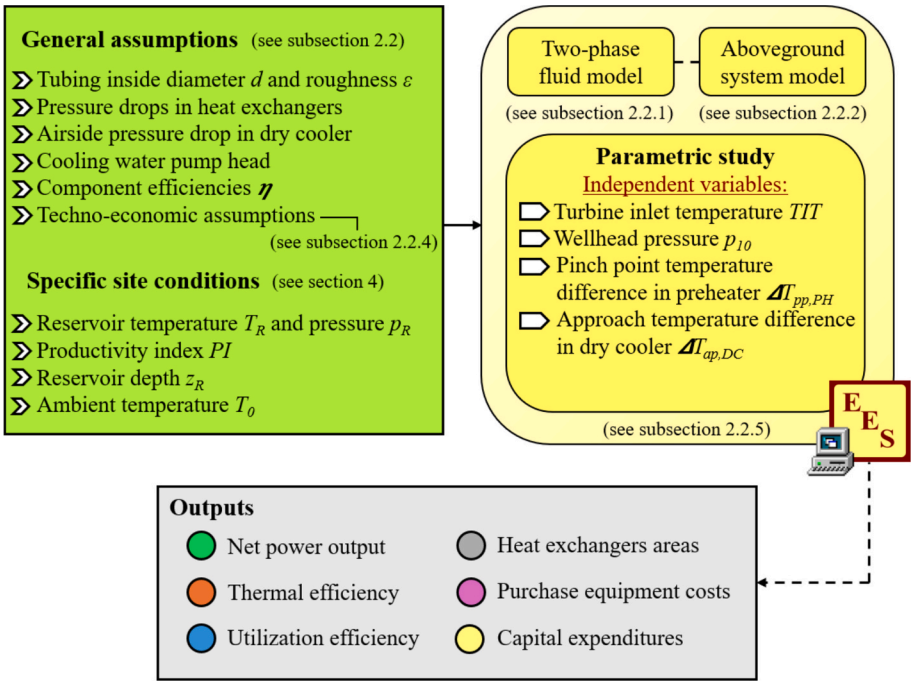

Fig. 3. Schematic representation of the methodology followed to obtain the output parameters.

The energy conservation in the geothermal fluid between the bottom-hole (state 9) and the wellhead (state 10) is applied through the Bernoulli equation, Eq. (2), where p is pressure, ϱ is density, g is gravity, z is elevation and v the fluid velocity:

$$p + \varrho g z + \frac{1}{2}\varrho v^2 = \text{constant} \tag{2}$$

The frictional pressure loss is taken into account when applying the Bernoulli equation and is calculated based on the frictional pressure gradient [49], Eq. (3), where f_m is the Moody friction factor for two-phase mixtures (dimensionless), v_m is the velocity of the steam/liquid mixture in m/s, ϱ_m is the mixture density in kg/m^3 and d is the tubing inside diameter in m:

$$-\left(\frac{dp}{dz}\right) = \frac{f_m \cdot v_m^2 \cdot \varrho_m}{2d} \tag{3}$$

The mixture density is the mass-average-mixture density of the two phases, ϱ_{st} and ϱ_l, and is therefore dependent on the vapor quality x:

$$\varrho_m = \varrho_{st} \cdot x + \varrho_l \cdot (1 - x) \tag{4}$$

The *Chen* equation [56] is used to calculate f_m, Eq. (5), where ε is the pipe roughness in m, Re_m is the Reynolds number (dimensionless), Eq. (6), and Λ is the roughness parameter (dimensionless), Eq. (7):

$$f_m = \frac{1}{\left[4\log\left(\frac{\varepsilon/d}{3.7065} - \frac{5.0452}{Re_m}\log\Lambda\right)\right]^2} \tag{5}$$

$$Re_m = \frac{d \cdot v_m \cdot \varrho_m}{\mu_m} \tag{6}$$

$$\Lambda = \frac{(\varepsilon/d)^{1.1098}}{2.8257} + \left(\frac{7.149}{Re_m}\right)^{0.8981} \tag{7}$$

For calculation of the Reynolds number, the mass-average-mixture viscosity is used, μ_m, in kg/(m·s):

$$\mu_m = \mu_{st} \cdot x + \mu_l \cdot (1 - x) \tag{8}$$

The drop in pressure of the two-phase fluid during its ascent induces the process of flashing [57], which is considered to be isenthalpic because it occurs steadily, without any heat transfer and with no work involvement [57]. Fig. 4 shows the hyperbolic curve of the isenthalpic process. In the curve, the increase in vapor quality during the flashing process can be observed, showing how hot-water geothermal wells flash to steam-water mixtures [58]. The value of the vapor quality can be determined from the wellhead pressure [57]. Assuming a direct connection between wellhead and separator, any pressure loss between them can be considered negligible [47]. The properties of pure liquid water are taken as a reference in this model for the geothermal liquid [35].

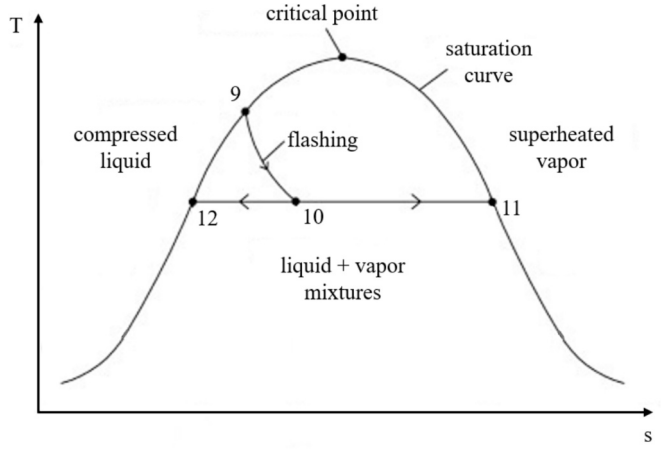

Fig. 4. Flashing on temperature–entropy diagram. Note: depending on each case, state 9 can correspond to saturated liquid, as represented in this figure, but also as compressed liquid, or a liquid–vapor mixture.

2.2.2. Aboveground system modelling

Thermodynamic equations are defined based on the law of conservation of energy. In this sense, Eq. (9) [59] represents the mechanical power developed in the adiabatic expansion process in the turbine $\dot{W}_T$, in kW, which depends on the mass flow rate of the working fluid $\dot{m}_{wf}$, in kg/s, and the enthalpy drop across the turbine, in kJ/kg:

$$\dot{W}_T = \dot{m}_{wf} \cdot (h_1 - h_2) \tag{9}$$

State 2 is determined through the isentropic efficiency of the turbine, Eq. (10) [47], where the subscript s refers to isentropic and therefore the process 1–2 s considers that 100% of the energy can ideally be transformed [59], while the real process 1–2 takes into account the irreversibilities:

$$\eta_{s,T} = \frac{h_1 - h_2}{h_1 - h_{2s}} \tag{10}$$

Energy balance in the recuperator:

$$\dot{m}_{wf} \cdot (h_2 - h_3) = \dot{m}_{wf} \cdot (h_6 - h_5) \tag{11}$$

The heat rejected by the working fluid in the condenser is:

$$\dot{Q}_C = \dot{m}_{wf} \cdot (h_3 - h_4) \tag{12}$$

This heat transfer explains the increase in temperature experienced by the cooling water in the condenser and, consequently, the air in the dry cooler. Eq. (13) represents the energy balance in the dry cooler, where T_{18} and T_{19} correspond to the temperatures of the cooling water at the inlet and outlet of the dry cooler, and T_{20} and T_{21} to the temperatures of the air at the inlet and outlet of the dry cooler, respectively:

$$\dot{m}_{CW} \cdot cp_{CW} \cdot (T_{18} - T_{19}) = \dot{m}_a \cdot cp_a \cdot (T_{21} - T_{20}) \tag{13}$$

The power supplied by the process pump to the working fluid is:

$$\dot{W}_P = \dot{m}_{wf} \cdot (h_5 - h_4) \tag{14}$$

Eq. (15) [47] represents the isentropic efficiency of the pump, from which state 5 is determined:

$$\eta_{s,P} = \frac{h_{5s} - h_4}{h_5 - h_4} \tag{15}$$

Energy balance in the preheater:

$$\dot{m}_{15} \cdot (h_{15} - h_{16}) = \dot{m}_{wf} \cdot (h_7 - h_6) \tag{16}$$

Energy balance in the evaporator E_A:

$$\dot{m}_{11} \cdot (h_{11} - h_{13}) = \dot{m}_{wf} \cdot (h_1 - h_8) \tag{17}$$

Energy balance in the evaporator E:

$$\dot{m}_{14} \cdot (h_{14} - h_{15}) = \dot{m}_{wf} \cdot (h_8 - h_7) \tag{18}$$

Eq. (19) [47] represents the quality of the mixture at the inlet of the separator, state 10:

$$x_{10} = \frac{h_{10} - h_{12}}{h_{11} - h_{12}} \tag{19}$$

2.2.3. Thermodynamic analysis

Eq. (20) [59] represents the ORC thermal efficiency, η_{th}, where $\dot{Q}_{in}$ is the total heat transferred by the geothermal fluid to the working fluid:

$$\eta_{th} = \frac{\dot{W}_T - \dot{W}_P}{\dot{Q}_{in}} = \frac{\dot{W}_T - \dot{W}_P}{\dot{m}_{wf}(h_1 - h_6)} \tag{20}$$

The net plant power output $\dot{W}_{net}$ is obtained as follows [47]:

$$\dot{W}_{net} = \dot{W}_G - \dot{W}_{aux} \quad (21)$$

where $\dot{W}_G$ is the gross electrical plant power output, Eq. (22), and $\dot{W}_{aux}$ is the auxiliary power consumption, which includes the electrical power consumed by the working fluid pump, the cooling water pump, and the dry cooling system fans (see assumed component efficiencies in Table 1).

$$\dot{W}_G = \dot{W}_T \cdot \eta_{mec,T} \cdot \eta_{el,G} \quad (22)$$

The utilization efficiency η_u, Eq. (23) [47], is based on the second law of thermodynamics and is a universal metric for the performance of power plants [30]. It is expressed as the ratio of the net plant power output (in kW) to the maximum exergy rate $\dot{E}_R$ (in kW), Eq. (24) [47], obtainable from the geothermal fluid in the reservoir state:

$$\eta_u = \frac{\dot{W}_{net}}{\dot{E}_R} \quad (23)$$

$$\dot{E}_R = \dot{m}_{gf}[h_R - h_0 - T_0 \cdot (s_R - s_0)] \quad (24)$$

where $\dot{m}_{gf}$ is the mass flow rate of the geothermal fluid (in kg/s), h is the specific enthalpy (in kJ/kg), s the specific entropy (in kJ/kg·K), and T the temperature (in kelvin). The subscript R refers to the condition of the geothermal fluid in the reservoir and the subscript 0 to the ambient conditions or the dead-state. The values of h_0 and s_0 are considered to be equal to the saturated liquid values at T_0 [47].

The exergy destruction rate of each component $\dot{E}_D$, Eq. (25) [59], assuming steady state and a single inlet and oputlet is calculated as follows:

$$\dot{E}_D = \dot{m}_{wf} T_0 \left[(s_o - s_i) + \frac{q_k}{T_k} \right] \quad (25)$$

where subscripts o and i refer to the condition of the working fluid at the outlet and inlet of the component, respectively. q_k corresponds to heat transferred from each heat source to the working fluid and T_k to the temperature of each heat source [59]. For the latter, the arithmetic mean temperature of the inlet and outlet temperatures of the heat source is taken. For the particular case of the condenser, the arithmetic mean temperature of the condenser inlet and condenser outlet temperatures of the cooling water is taken [59].

2.2.4. Economic analysis

In addition to analyzing the thermodynamic performance of the geothermal system, it is necessary to evaluate the effect of the proposed design on the plant's economic performance. To this end, the original purchased equipment costs (PECs) of the ORC are first calculated using the equations presented in Table 2. The original PEC of the additional evaporator E_A is calculated using Eq. (26) [60], corresponding to that of a falling-film evaporator, which is characterized by operating with heating steam outside the tubes. Similarly, the original PECs of the heat rejection system are calculated using Eq. (27), corresponding to the cooling water pump [60], and Eq. (28), corresponding to the dry cooler [60]. In this study, the US dollar to euro exchange rate as of July 31, 2025, [61] was applied to the resulting PECs.

$$\log_{10}(PEC_{EA}) = 3.9119 + 0.8627 \cdot \log_{10}(A_{EA}) - 0.0088 \cdot [\log_{10}(A_{EA})]^2 \quad (26)$$

$$\log_{10}(PEC_{CP}) = 3.3892 + 0.0536 \cdot \log_{10}\left(\dot{W}_{CP}\right) + 0.1538 \cdot [\log_{10}(\dot{W}_{CP})]^2 \quad (27)$$

where $\dot{W}_{CP}$ is the shaft power of the cooling water pump in kW.

$$\log_{10}(PEC_{DC}) = 4.0336 + 0.2341 \cdot \log_{10}(A_{DC}) + 0.0497 \cdot [\log_{10}(A_{DC})]^2 \quad (28)$$

The Chemical Engineering Plant Cost Index (CEPCI) [62] was used to update the original PECs to the reference year, Eq. (29). The CEPCIs for the original year are shown in Table 2. The PECs calculated from Eq. (26), Eq. (27) and Eq. (28) are subject to an original CEPCI of 397 [60].

$$PEC_{ry} = PEC_{oy} \cdot \frac{CEPCI_{ry}}{CEPCI_{oy}} \quad (29)$$

where subscripts *ry* and *oy* correspond to the reference year and original year, respectively. In this study, a $CEPCI_{ry}$ of 817.8 is assumed, which corresponds to the most recent official CEPCI value [62].

The total capital investment (CI) is the sum of the total PEC at the reference year, well costs, and other direct costs. For this study, the cost per well was assumed to be 350 €/kW [63] (applying the US dollar to euro exchange rate as of 31 July 2025 [61]). Among the direct costs are those related to piping, assumed to be 7% of PEC [64], and other expenses related to a power plant construction (e.g., working fluid costs and installation of equipment), assumed to be 6% of the PEC [64]. The CAPEX, in €/kW, was calculated by dividing the total CI of the geothermal plant by its net power output.

- Heat exchanger area and the effect on the PEC

The heat transfer surface area of the heat exchangers will determine the PEC of these components (see Table 2). The simple mathematical method based on the mean temperature difference concept is used to calculate the area required to transfer a given heat flow rate, Eq. (30) [65]:

$$A = \frac{\dot{Q}}{U \cdot \Delta T_{LM}} \quad (30)$$

where A is the area in m^2, $\dot{Q}$ is the heat flow rate in W, U is the local overall heat transfer coefficient in $W/m^2 \cdot K$, and ΔT_{LM} is the logarithmic mean temperature difference in K. Eq. (31) represents calculation of the logarithmic mean temperature difference, where ΔT_1 and ΔT_2 are the temperature differences between the two fluids, evaluated at the terminals of the equipment [66]:

$$\Delta T_{LM} = \frac{\Delta T_1 - \Delta T_2}{\ln\left(\frac{\Delta T_1}{\Delta T_2}\right)} \quad (31)$$

In the limiting case of $\Delta T_1 \rightarrow \Delta T_2$, the logarithmic approaches the arithmetic mean, Eq. (32) [65]. This equation is applied particularly for the evaporator E_A, given that in this latent heat is only transferred from the geothermal fluid in vapor state to the working fluid, also in vapor state:

Table 2
Cost equations of diverse equipment used in the ORC.

Component	PEC	CEPCI	Reference
Preheater	$130 \cdot (A_{PH}/0.093)^{0.78}$	550.8	[93]
Evaporator E	$130 \cdot (A_E/0.093)^{0.78}$	550.8	[93]
Recuperator	$130 \cdot (A_R/0.093)^{0.78}$	550.8	[93]
Turbine	$6000 \cdot \left(\dot{W}_T\right)^{0.7}$	397	[94]
Condenser	$1773 \cdot \dot{m}_{wf}$	468.2	[93]
Process pump	$3540 \cdot \left(\dot{W}_P\right)^{0.7}$	468.2	[93]
Generator	$60 \cdot \left(\dot{W}_G\right)^{0.95}$	397	[94]

$$\Delta T_{LM} = \frac{1}{2}(\Delta T_1 + \Delta T_2) \quad (32)$$

Heat exchangers constitute a large proportion of the investment cost of an ORC installation [67]. However, it is difficult to reliably determine the overall heat transfer coefficients without experiments [68]. For these reasons, this study includes a sensitivity analysis to assess the impact of the overall heat transfer coefficients on the resulting area and capital cost of the different types of heat exchanger. For this purpose, different U-value ranges available in the literature for the evaporators, preheater, recuperator, condenser, and dry cooler were used as reference ranges. Table 3 presents the heat transfer conditions and typical U-value ranges for different types of heat exchanger.

2.2.5. Parametric study

A parametric study was conducted to assess the influence of different process and component design parameters on system performance. One of the selected process design parameters is the turbine inlet temperature (TIT), given its direct influence on the thermal efficiency and net power output of the system. In addition, given the dependency of the mass flow rate on the wellhead pressure [43], the latter was selected as an operating parameter. The temperature differences in two heat exchangers were chosen as component design parameters, as they influence both the net power output and the required heat transfer areas of these devices. More specifically, these are the pinch point temperature difference in the preheater, $\Delta T_{pp,PH}$, which is the minimum temperature difference between the geothermal fluid and the working fluid, and the approach temperature difference in the dry cooler, $\Delta T_{ap,DC}$, which is the temperature difference between the cooling water at the dry cooler outlet, T_{19}, and the air at the dry cooler inlet, T_{20}.

The parametric study adopts an optimization approach based on the *Min/Max* command of EES [69]. The application procedure of this command is detailed in the following steps:

The syntax of the equations is checked (automatic check of EES).
The variable to be maximized or minimized is defined.
The independent variables whose values will be changed in the search for the optimum are selected.
The lower and upper bounds of the selected independent variables are defined.
The execution of the algorithm is ordered to obtain the values of the independent variables for which the defined dependent variable is optimized.

In this study, after checking the syntax of the equations (Step 1), the net power output was defined as the variable to be maximized (Step 2). Subsequently, the TIT, the wellhead pressure, the pinch-point temperature difference in the preheater, and the approach temperature difference in the dry cooler were selected as independent variables (Step 3). Then, the lower and upper bounds of the independent variables were specified as shown in Table 4 (Step 4). Having selected more than one independent variable, EES uses Brent's method [70] to determine the maximum value of the target variable [69] (Step 5). After the simulation, all the parameters were obtained corresponding to the optimal design of the system which maximizes the net power output of the plant, hereinafter referred to in this paper as the power optimum design (POD).

The simulation process was developed for the different working fluids selected, as described in the following subsection.

2.2.6. Selected working fluids

The process design analysis was conducted for three retrograde organic fluids commonly used in ORC geothermal plants: n-pentane, isopentane, and n-butane. Their main properties are shown in Table 5. Technical and environmental aspects were taken into account in their selection as working fluid candidates. In terms of technical aspects, n-pentane and isopentane were selected for their high performance in high-temperature ORC applications [71], while n-butane was also included as one of the best options, especially for low- to medium-temperature applications [72]. Furthermore, all three meet the condition of being retrograde fluids, which ensures dry expansion in the turbine. They were also selected for being environmentally friendly fluids, since all three have zero ozone depletion potential (ODP) and a very low global warming potential (GWP) (see Table 5). In terms of safety, it should be noted that all three candidates are highly flammable, as are most working fluids used in commercial ORC systems, while in terms of health, only one of them—isopentane—is considered toxic.

The fluid property information provided by EES [48] was used, which offers highly accurate thermodynamic and transport properties for the aforementioned organic fluids, obtained from their fundamental equations of state (EOS).

2.2.7. Validation

To validate the model's behavior, a reference geothermal system was identified and analyzed using available data from the literature. More specifically, the energy balance equations adapted to the reference system were solved using the same input parameters as in [73], most of which are real data from an existing plant. These are the enthalpy, temperature, and pressure of the geofluid at the separator inlet: 1379.7 kJ/kg, 187 °C, and 10.5 bar, respectively. The steam and brine mass flow rates are 48 and 110.6 kg/s, respectively, the ambient conditions are 18 °C and 0.78 bar, and the reservoir temperature is 306 °C. After the simulation, small variations in the results obtained in [73] and those in this study were observed, with a difference of +0.97% for net power output and +1.09% for utilization efficiency (see Table 6), which verifies the model's predictive capability.

2.3. Techno-economic comparison

The thermodynamic and economic results obtained with the proposed ORC system in this study were then compared with those obtained by other reference geothermal systems under the same geothermal fluid conditions, both in the reservoir and at the wellhead. Specifically, the reference geothermal systems selected for comparison are a

Table 3
Conditions of heat transfer and typical U-value range for the different types of heat exchanger.

Heat exchanger	Conditions of heat transfer	U (W/m^2·K)	Reference
Evaporator E	Heating water outside the tubes to evaporate low viscosity organic fluids	600–1700	[95]
Evaporator E_A	Heating steam outside the tubes to evaporate low viscosity organic fluids	2000–4000[a]	[96]
Preheater	Liquid on the shell and tube sides	150–1200	[95]
Recuperator	Organic solvent on the shell and tube sides	200–500	[97]
Condenser	Cooling water on the tube side and organic vapor on the shell side	300–1200	[95]
Dry cooler	Water as hot fluid and air as cold fluid	400–600	[97]

[a] Falling-film evaporator.

Table 4
Independent variables selected and their respective established bounds.

Independent variable	Bounds
Wellhead pressure	$12 \leq p_{10}$ (bar) ≤ 20[a]
Turbine inlet temperature (TIT)	($T_{critical}$-50) $\leq$ TIT (°C)$\ll T_{critical}$[b]
Pinch point temperature difference in the preheater	$5 \leq \Delta T_{pp,PH}$ (°C) ≤ 15
Approach temperature difference in dry cooler	$10 \leq \Delta T_{ap,DC}$ (°C) ≤ 25[c]

[a] Range established based on the well productivity curve (see section 4).
[b] Subcritical ORC [91].
[c] Range established in accordance with a regulatory test procedure [52].

Table 5
Physical, environmental, and health and safety properties of the candidate working fluids [47,71].

Working fluid	$T_{critical}$ (°C)	$p_{critical}$ (bar)	$\varrho_{critical}$ (kg/m^3)	ODP	GWP	Flammability	Toxicity
n-pentane	196.6	33.6	231.60	0	3	Highly flammable	Low
isopentane	187.2	33.8	235.92	0	11	Highly flammable	Toxic
n-butane	152.0	38.0	227.83	0	3	Highly flammable	Acceptable

Table 6
Validation of the developed model.

Performance parameter	Ref. [73]	Present study[a,b,c]
Available exergy rate (kW)	66,204	66,168
Net power output (kW)	24,300	24,535
Utilization efficiency (%)	36.7	37.1

[a] Turbine inlet (saturated vapor) and outlet enthalpies of 2778.1 and 2167.4 kJ/kg, respectively.
[b] Condenser inlet and outlet (saturated liquid) enthalpies of 2167.4 and 175.9 kJ/kg, respectively.
[c] Gross power output: 27,849 kW; auxiliary power consumption: 3314 kW.

conventional single-flash system and a combined flash-binary system. The description and layout of the single-flash system and the flash-binary system are presented in [73] and [34], respectively. For the comparison, the same geothermal fluid temperature before reinjection (state 16) was considered. Likewise, the same organic working fluid and pinch-point temperature difference in the preheater were considered for the proposed ORC system and the flash-binary cycle. The output parameters to be compared were the net power output, SPO, utilization efficiency, and the CAPEX.

3. Case study description

A region located on the island of Tenerife was chosen for the case study of this paper. This island is one of the Canary Islands (Spain), a volcanic archipelago located in the Atlantic Ocean, off the coast of West Africa (see Fig. 5). With an area of 2034 m^2 and a population of 965,575 inhabitants in 2025 [74], Tenerife is the largest and most populated island in the archipelago and additionally welcomed more than 7.3 million tourists in 2024 [75]. The island's electrical system is isolated, with no interconnection with other islands or the mainland. It had an installed capacity of 1441 MW in 2023, of which 75.4% corresponded to conventional thermal generation plants [76]. The rest of the configuration park corresponds to renewable generation technologies, with wind power predominating with 63.9% of the installed renewable capacity, followed by solar PV with 35.2%. Gross electricity production amounted to 3677 GWh in 2023, with 18.9% originating from renewable sources, while the net peak power demand was 585 MW [76]. The need to decarbonize positions Tenerife, as well as the other Canary Islands, in a medium-term context of high renewable power integration [77]. In this regard, energy storage systems will be required to manage the fluctuating nature of the non-dispatchable renewable resources, as well as dispatchable generation modules.

Geothermal energy is a clear candidate as a dispatchable renewable source for Tenerife. Of all the islands in the archipelago, Tenerife has the highest degree of maturity in terms of the exploration of this resource, making it the priority island for the conducting of geothermal research drillings in order to confirm its potential for energy exploitation [78]. In the 1990 s, the Geological and Mining Institute of Spain (IGME by its initials in Spanish) conducted geothermal research in Tenerife [79]. Their analysis of geothermal indicators showed a correlation between areas with the highest geochemical anomalies and tectonic-volcanic fractures, which increases the likelihood of the existence of geothermal deposits. Regarding temperature, the IGME conducted a preliminary analysis of its distribution and detected the highest concentration of anomalous points in the southern part of the island. In this area, anomalies of silica and ammonia were also detected, with gases present, from which the presence of deep fractures that act as escape routes for volatile components can be deduced. The IGME carried out an application of geothermometry but did not consider the results obtained to be interpretable.

Geothermal research on the island was resumed in 2011 through the GEOTHERCAN project [80], the objective of which was the experimental development of 3D models for the characterization of

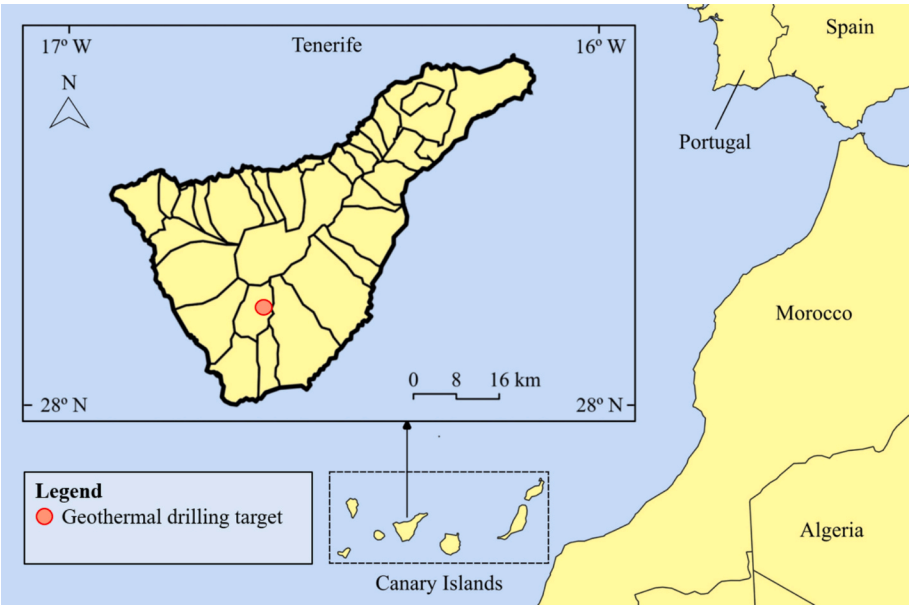

Fig. 5. Geographical location of the island of Tenerife and the geothermal drilling target in the town of Vilaflor.

geothermal deposits in the subsoil of the Canary Islands. The main collaborating entities in the project were the Institute for Technology and Renewable Energies (ITER) [81], Petratherm Limited [82], and the Volcanology Institute of the Canary Islands (INVOLCAN) [83]. Through 3D inversion modeling of an extensive magnetotelluric survey, a drilling target was identified on the southern slopes of Teide Volcano, near the town of Vilaflor (see Fig. 5) [84]. The site was targeted based on the detection of the thinning of a clay cap [84], which can be indicative of geothermal alteration occurring just above the resource [85]. A geothermal upwelling zone is therefore anticipated, with a 2000-meter drill being sufficient to penetrate the clay cap and reach the geothermal reservoir. A geochemical analysis indicated that the reservoir is liquid-dominated, with a temperature of approximately 240 °C [84,86]. From the application of geobarometry, a reservoir pressure of 42 bar is expected [87]. According to [86], the drilling of eight production wells of 2000 m in length is planned at the target site. It should be noted that this area is within the *Garehagua II* mining license, which showed the highest potential to contain geothermal resources based on the geochemical indicators obtained in an exploration of deep-seated geothermal reservoirs through soil CO_2 degassing surveys [88].

The Vilaflor target site was selected as case study for this paper as it is identified in the strategic document on geothermal energy in the Canary Islands [78] as a priority area for geothermal energy development and exhibits the highest level of exploratory maturity of the resource in the archipelago. This advanced stage of geothermal exploration offers high levels of reliability in terms of reservoir condition estimates, including temperature, pressure, and depth—parameters that are fundamental given their direct influence on the design and performance of the geothermal power plant. As for the PI, an average value of 20 l/(s·bar) [55] was assumed for this case as test drilling has not yet been conducted in the study area. For this last reason, no reliable data on NCGs are currently available, and consequently the range of possible gas compositions is quite large. Therefore, stream 11 is assumed to be pure steam in this study, and the effects of NCGs on the performance of the steam-condensing evaporator are not considered. These effects should be addressed in future research studies, once the maturity of geothermal exploration allows the composition of non-condensable gases to be properly characterized. Likewise, corrosion in heat exchangers and the piping system caused by the acidic solution formed by the dissolution of H_2S and CO_2 in the condensate should also be considered. Preventing corrosion requires corrosion-resistant material, such as stainless steel, or a protective coating.

It should also be noted that in the cited strategic document [78] the ORC is considered the priority technology to be installed in the archipelago, given its high reliability, flexibility, and environmental performance. For this reason, this geothermal technology for electricity production was selected for the case study in this paper.

4. Results and discussion

The results presented and analyzed in this section were obtained under the assumption of the following input parameters considered for the particular case of this paper (see section 3):

(1) A reservoir temperature and pressure of 240 °C and 42 bar, respectively.
(2) A productivity index (PI) of 20 l/(s·bar).
(3) Eight production wells of 2000 m in length.
(4) An ambient temperature of 25 °C.

Fig. 6 represents the resulting productivity curve for a single geothermal well in terms of the mass flow rate of the two-phase fluid as a function of the wellhead pressure. In the curve, it can be seen that when the valve is closed the mass flow rate of the mixture is zero and the wellhead pressure is at its maximum. In contrast, when the valve is opened the flow increases rapidly and the wellhead pressure is lowered.

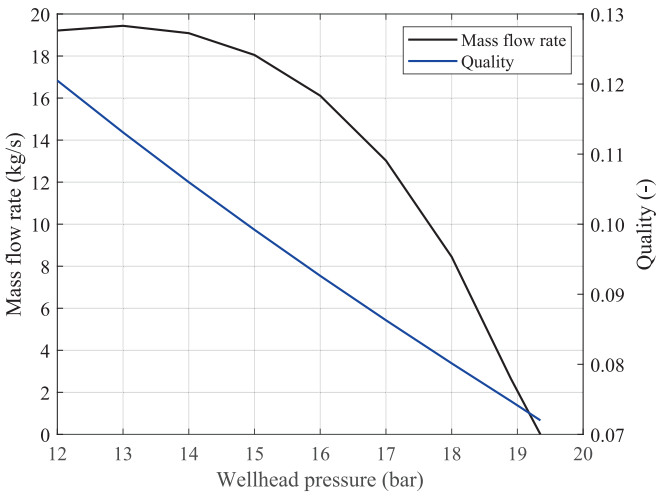

Fig. 6. Geothermal well productivity curve and quality of the two-phase fluid.

Just like the mass flow rate, the vapor quality also increases when the pressure is reduced. The mass flow rate of the two-phase mixture is maximum for a wellhead pressure of 13 bar, reaching 19.4 kg/s as a result of a difference between the initial static pressure in the reservoir and the flowing bottom-hole pressure at the well of 17.6 bar. Under these conditions, the mixture velocity, density, and viscosity at the wellhead are 8.7 m/s, 55.2 kg/m^3, and 0.000126 kg/(m·s), respectively. The frictional pressure gradient is $0.2862 \cdot 10^{-3}$ bar/m. The total mass flow rates extracted through the eight wells amount to 137.9 and 17.6 kg/s of liquid and steam, respectively, corresponding to a vapor quality of 11.3% at the separator inlet. Table 7 shows the thermodynamic properties of the geothermal fluid, from the reservoir to its reinjection, with a wellhead pressure of 13 bar.

The effect of the TIT on the net plant power output is represented in Fig. 7a. For the three working fluids, both the net power output and the thermal efficiency increase with the rise in TIT and reach a maximum at a specific TIT. More specifically, the net power output is maximized for TITs of 175.0 °C, 168.2 °C and 141.1 °C with n-pentane, isopentane and n-butane, respectively. The drop in net power output given with TIT values close to the critical temperature is due to the additional efficiency losses in the expansion process related to the flow conditions. Fig. 7b shows the influence of the wellhead pressure on the net power output, assuming the optimum TIT for each working fluid. It can be seen that the wellhead pressure of 13 bar is the operating point that maximizes the net power output for the three working fluids considered. That point corresponds to the separator temperature of 191.6 °C (see Table 7) and an available exergy rate of 36,894 kW. Table 8 shows, for the three working fluids, the net power output, thermal efficiency and utilization efficiency achieved in the POD scenario. n-pentane achieves the highest net power output, thermal efficiency and utilization efficiency of the system. It should also be noted that, of the three working fluids considered, n-pentane has the highest critical temperature, which offers a greater

Table 7
Thermodynamic properties of the geothermal fluid for a wellhead pressure of 13 bar.

State	T (°C)	p (bar)	h (kJ/kg)	x (–)
9	222.7	24.40	1037.4	0.044
10	191.6	13.00	1037.4	0.113
11	191.6	13.00	2786.5	1
12	191.6	13.00	814.6	0
13	190.7	12.74	810.5	0
14	191.5	12.97	814.1	0
15	185.5	12.71	787.5	—[a]
16	87.8	12.46	368.8	—[a]

[a] Not applicable for subcooled liquid.

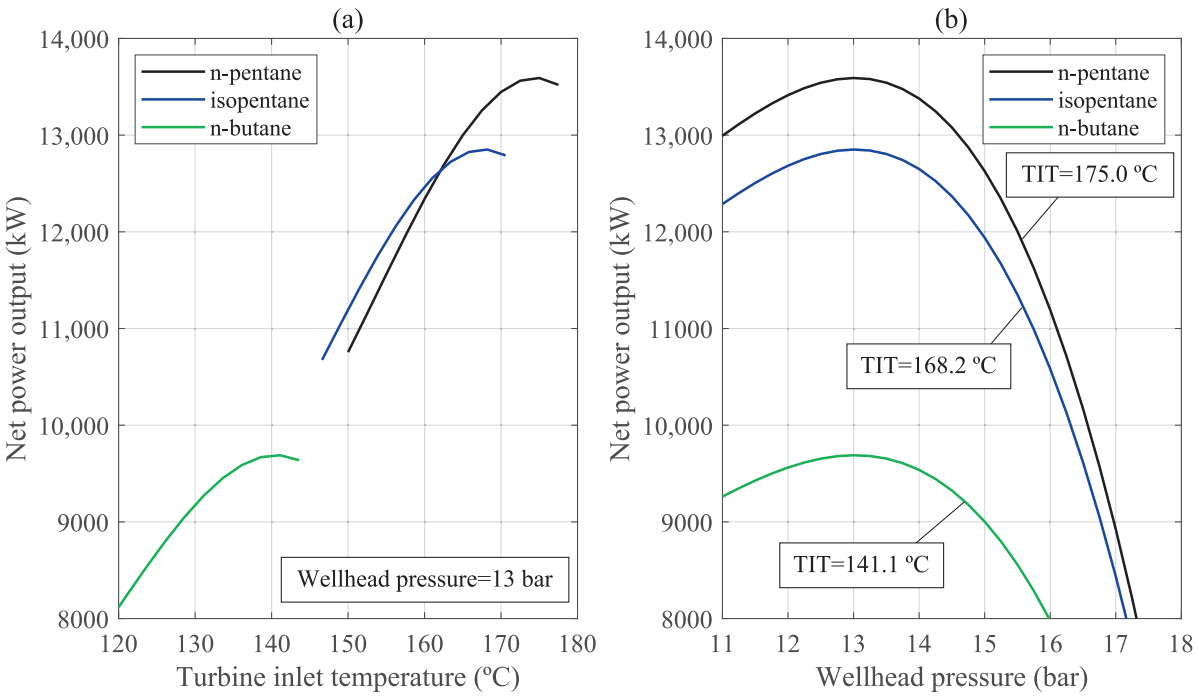

Fig. 7. Net power output vs. turbine inlet temperature (TIT) (a) and wellhead pressure (b).

Table 8
Net power output, thermal efficiency and utilization efficiency in the POD scenario for each working fluid.

Working fluid	$\dot{W}_{net}$ (kW)	η_{th} (%)	η_{lu} (%)
n-pentane	13,591	18.3	36.8
isopentane	12,851	17.3	34.8
n-butane	9689	12.4	26.3

margin to increase the TIT. In addition to greater performance, n-pentane has lower GWP and toxicity than isopentane (see Table 5). Together, these characteristics suggest that n-pentane is the most appropriate working fluid for the case study presented in this paper from a technical, environmental, and health and safety perspective.

The decrease in the pinch point temperature difference in the preheater corresponds with a lower slope of curve 6–7 in the temperature-heat transfer diagram (see Fig. 8). This results in a higher heat capacity rate, and consequently, a higher net power output. The latter is maximized for the minimum pinch point temperature difference considered for this analysis (5 K). Conversely, the net power output decreases linearly with the increase in the pinch point temperature difference. Note that for the entire range considered for the pinch point temperature difference, namely from 5 to 15 K, the pinch point occurs between states 16 and 6, that is, at the cold end of the preheater.

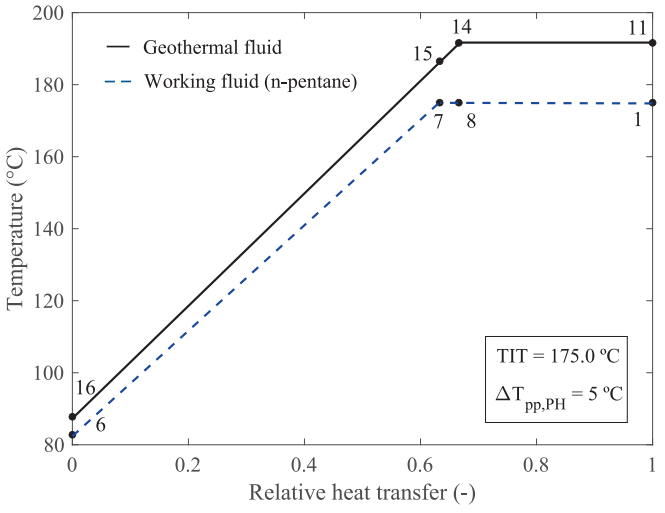

Fig. 8. Temperature-relative heat transfer diagram for the preheater and evaporators.

This pinch point location is not common in geothermal applications with ORC, given that it is normally located at the bubble point [47]. According to DiPippo [47], while it is theoretically possible for the pinch point to occur at the cold end of the preheater (for a very steep brine cooling line), this practically never happens. This is because a medium or low-temperature geothermal fluid is commonly used, which only transfers sensible heat from its entry into the evaporator to its exit from the preheater. In contrast, in the case study of this paper, a two-phase flow is used, whose vapor state part is condensed in the E_A evaporator, resulting in a greater temperature difference between the geothermal fluid and the working fluid at the hot end of the preheater, thus shifting the pinch point to the cold end.

The effect of the approach temperature difference in the dry cooler on the power output of the plant is shown in Fig. 9. The net power output is maximized for an approach temperature difference in the dry cooler of 16 K, as shown in Fig. 9a. On the one hand, as can be seen in Fig. 9b, as the approach temperature difference decreases, the gross electrical power of the plant increases due to the rise in the thermal efficiency of the cycle. However, the air flow rate also increases, leading to higher energy consumption by the fans. This last point justifies the increase in the share of auxiliary power requirements to gross power output, which rises to 38.6% for an approach temperature difference of 10 K in the dry cooler.

Table 9 shows the thermodynamic properties of n-pentane obtained for the POD point corresponding to a TIT of 175 °C, a wellhead pressure of 13 bar, a pinch point temperature difference in the preheater of 5 K, and an approach temperature difference in the dry cooler of 16 K. Under these conditions, the total mass flows required for cooling water and air are 4111 and 7772 kg/s, respectively. The mass flow rate of n-pentane is 234.65 kg/s. Table 10 shows the thermodynamic properties of cooling

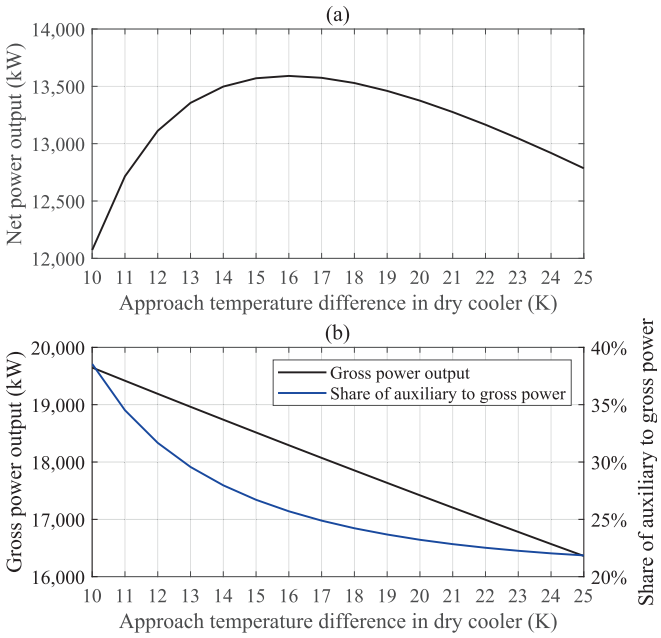

Fig. 9. Effect of the approach temperature difference in the dry cooler on the net power output (a) and on the gross power output and the share of auxiliary power needs to gross power output (b). Note: working fluid: n-pentane; TIT = 175 °C; p_{10} = 13 bar; $\Delta T_{pp,PH}$ = 5 °C.

Table 9
Thermodynamic properties of n-pentane in the POD scenario.

State	T (°C)	p (bar)	h (kJ/kg)	s (kJ/kg·K)
1	175.0	24.12	560.62	1.400
2	99.2	1.71	474.24	1.441
3	62.3	1.68	402.16	1.240
4	51.0	1.64	35.98	0.113
5	52.3	26.15	41.12	0.116
6	82.8	25.63	117.54	0.341
7	177.6	25.11	405.23	1.052
8	176.3	24.61	418.89	1.083

Table 10
Thermodynamic properties of cooling water and air in the POD scenario.

Stream	T (°C)	p (Pa)
Cooling water		
17	41	248,475
18	46	101,325
19	41	101,325
Air		
20	25	101,325
21	36	101,125

water and air in the POD scenario. The gross electrical output of the plant amounts to 18,293 kW. The auxiliary power requirements correspond to 25.7% of the gross power output. More specifically, the power absorbed by the fans, process pump, and cooling water pump amounts to 2115 kW, 1723 kW, and 863.9 kW, respectively. The consumption of the fans represents a considerable share of the gross power output (11.6%).

Fig. 10 shows the exergy destruction rate of each component of the ORC and its corresponding contribution to the total exergy destruction rate of the ORC in the POD scenario. The highest exergy destruction rates occur in the turbine, condenser, recuperator, and the E_A evaporator. It was observed that, although increasing the TIT to 175 °C implies an increase in the exergy destruction rate of the turbine, it also implies a decrease in the exergy destruction rate of the evaporators and the

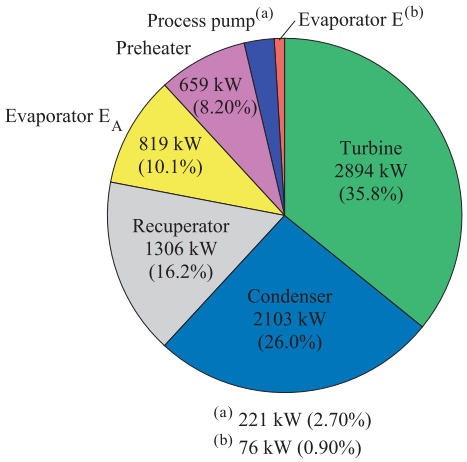

Fig. 10. Exergy destruction rate of each component of the ORC in the POD scenario.

preheater, resulting in a reduction in the total exergy destruction rate of the ORC and, consequently, an improvement in the overall exergetic efficiency.

The effect of the local overall heat transfer coefficient on the required area and capital cost of each type of heat exchanger is shown in Fig. 11. The heat flow rates in each heat exchanger considered for this sensitivity analysis correspond to those of the POD scenario. Across the entire considered range of U-values, the additional E_A evaporator exhibits the highest capital cost, despite requiring smaller heat transfer surface areas than the other heat exchangers. This is due to its greater design complexity compared to other conventional evaporator types, which significantly increases its capital cost. On the other hand, dry coolers always have total heat transfer surface areas exceeding 10,000 m^2. Likewise, their total capital cost would always exceed €1 million. However, the preheater could require similar surface areas and higher capital costs than dry coolers for U-values between 150 and 300 W/m^2·K. Specifically, the capital cost of the preheater with a U-value of 150 W/m^2·K is more than five times that of the same preheater with a U-value of 1200 W/m^2·K, illustrating the high sensitivity of the heat exchanger's area and economic cost to its respective local overall heat transfer coefficient. With respect to the recuperator, the total area and capital cost are significantly lower than those of the preheater or dry coolers, with an area always below 2000 m^2 and capital costs under €405,000. The heat transfer area required by the condenser would vary between 6605 and 1651 m^2, corresponding to U-values of 300 and 1200 W/m^2·K, respectively.

Fig. 12 shows the PEC of each ORC component in the POD scenario, assuming the average U-value for each type of heat exchanger. In this case, the total PEC of the ORC components would be €19,734,374. As can be seen, the turbine's PEC accounts for more than half (56.6%) of the total PECs, making it the most expensive component of the ORC. The additional steam-condensing E_A evaporator is the second most expensive component of the ORC, accounting for 17.9% of the total PECs. In this regard, harnessing separated geothermal steam entails a considerable economic overhead due to the high capital cost of the steam-condensing evaporator incorporated into the proposed ORC system. Taking into account the costs of the wells (€37,996,448), piping (€1,381,406), and other direct costs (€1,184,062), the total capital investment (CI) for the geothermal plant would amount to €60,296,290.

Table 11 shows the resulting net power output, SPO, utilization efficiency, and CAPEX for the proposed ORC system, a single-flash system, and a combined flash-binary system under the same geothermal conditions at the wellhead, which correspond to a temperature of 191.6 °C and a pressure of 13 bar. The ORC improves both net power output and SPO by up to 148% compared to the single-flash system. In this case, the

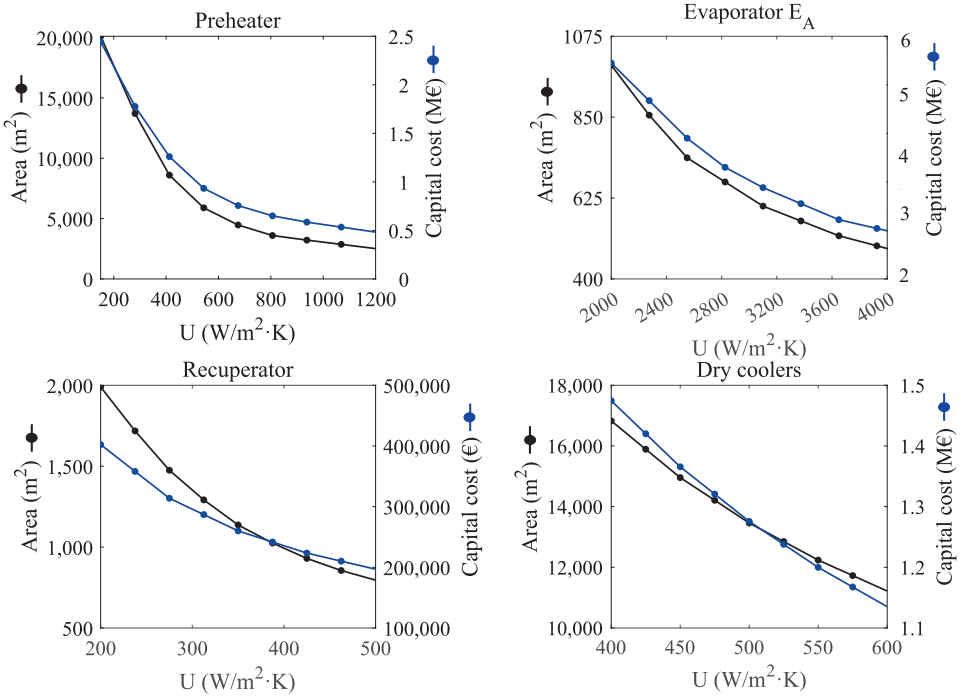

Fig. 11. Heat transfer area and capital cost of the heat exchangers as a function of the local overall heat transfer coefficient.

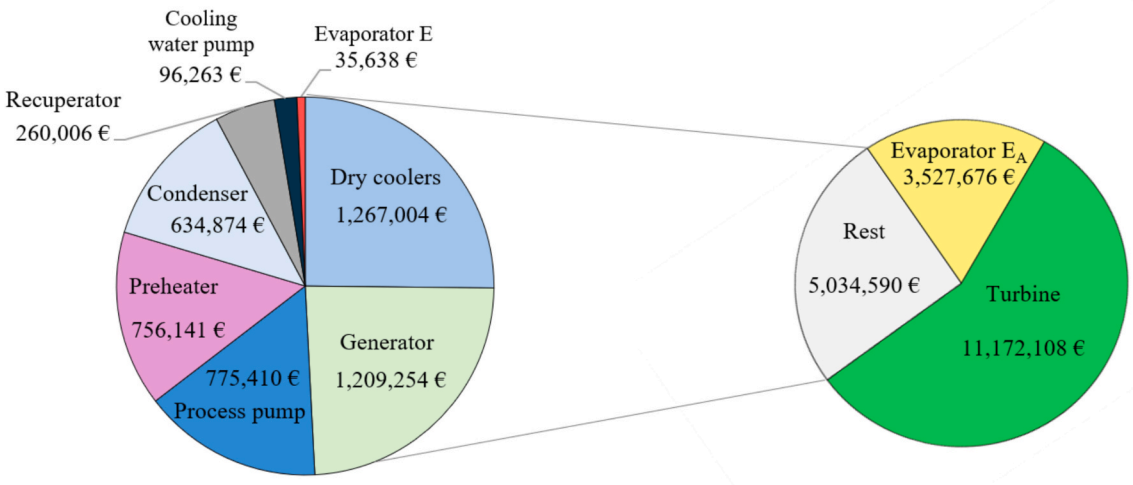

Fig. 12. PEC of each ORC component for the POD scenario.

low quality of the geothermal fluid in the separator results in a significant decrease in turbine work output and, consequently, in the power that the single-flash system could generate. For its part, the flash-binary system increases energy capture by also harnessing the heat released by the geothermal liquid to the working fluid of the incorporated binary cycle, improving both net power output and the SPO by 97.5% compared to the single-flash system. However, the ORC system improves both the net power output and the SPO achieved by the combined flash-binary cycle by 25.6%. With respect to utilization efficiency, the ORC system improves upon the single-flash and combined flash-binary systems by 22 and 7.5 percentage points, respectively.

In terms of economic aspects, the proposed ORC system has a CAPEX 5.6% higher than that of the single-flash system. This increase in CAPEX is more than offset by the improvement in the SPO. On the other hand, the ORC system reduces the resulting CAPEX for the flash-binary system by 19.2%.

As can be seen, the net power output of the geothermal system is significantly increased with the proposed ORC system under the POD scenario. Consequently, the system would be able to produce a greater amount of baseload electricity.

For the case study on the island of Tenerife, its electricity system requires the additional installation of 200 MW of dispatchable capacity by 2030 and 800 MW by 2040 due to the upcoming expiration of the regulatory lifespan of a significant portion of its conventional thermal power plants [77]. Geothermal energy is one of the priority solutions not based on fossil fuel use to replace part of the conventional thermal power to be decommissioned. In this regard, the incorporation of the proposed geothermal power plant would contribute favorably to the energy system, both by providing baseload electricity and by offering demand-response services, which are especially necessary in energy systems with a high share of non-dispatchable RES such as wind and solar PV. Geothermal energy could cover a significant part of the island's

Table 11
Comparison of the results obtained for the proposed ORC, single-flash and flash-binary systems.

Performance parameter	ORC proposed	Single-flash[a,b,c]	Flash-binary[d]
$\dot{W}_{net}$(kW)	13,591	5478	10,819
SPO (kW/(kg/s))[e]	87.4	35.2	69.6
η_{lu} (%)	36.8	14.8	29.3
CAPEX (€/kW)	4436.53	4200.76	5487.53

[a] Turbine inlet (saturated vapor) and outlet enthalpies of 2786.5 and 2364.9 kJ/kg, respectively.
[b] Condenser inlet and outlet (saturated liquid) enthalpies of 2364.9 and 367.9 kJ/kg, respectively.
[c] Gross power output: 7049.30 kW; auxiliary power consumption: 1218.48 kW.
[d] Net power output of the flash and binary cycles of 5478 and 5341 kW, respectively.
[e] Calculated as $\dot{W}_{net}/\dot{m}_{gf}$.

electricity demand while reducing fossil fuel dependency [89]. Furthermore, this generation technology replacement would be in line with the transition towards a more sustainable system, given that the current emission factor for conventional thermal generation in Tenerife's energy system is 675 $gCO_{2\text{-eq}}$/kWh [76], while geothermal generation using binary technology has an average value of 11.3 $gCO_{2\text{-eq}}$/kWh [90].

5. Conclusions

In the present paper, an original design for an ORC system is proposed to harness geothermal resources from high-temperature reservoirs. It is a non-standard plant concept, as it includes separation of the two-phase geothermal fluid and condensation of the separated steam to partially evaporate the organic working fluid, while the remaining evaporation and preheating are achieved through cooling of the condensate/brine mixture. A numerical model of the two-phase geofluid and the aboveground system is implemented to simulate the thermodynamic performance. The effect of different process and component design variables on the net plant power output is measured in a parametric study. The optimum design which maximizes net plant power output is determined and compared with other geothermal energy systems from a technoeconomic standpoint. The method was applied to a case study on the island of Tenerife, Spain.

It was found that system performance strongly depends on the wellhead pressure and the turbine inlet temperature (TIT). For the different working fluids considered, the net power output is maximized at a specific operating point, namely a wellhead pressure of 13 bar for the system proposed in this paper. The increase in TIT leads to an increase in net power output, although a slight power loss must be considered when it approaches the critical temperature. From the analysis, it is concluded that organic fluids with a higher critical temperature can achieve a greater net power output when using high-temperature geothermal resources.

With respect to the component design parameters, the results show that reducing the pinch point temperature difference in the preheater leads to an increase in the net power output. From the thermal analysis in the preheater, it is deduced that, unlike standard ORC applications, this pinch point shifts to the cold end of the heat exchanger due to the condensation process of the separated geothermal steam. On the other hand, the decrease in the approach temperature difference in the dry cooler increases both the gross power output and the auxiliary power requirements of the plant. In this regard, it is determined that, within the range of values considered for this design variable, a temperature difference of 16 K is the trade-off solution that maximizes the net power output of the plant designed for the case study of this paper.

The optimum ORC design exhibits a maximum net power output of 13.59 MW and a utilization efficiency of 36.8% when n-pentane is used as the working fluid. The novel design proposed in this study for the ORC system improves its specific power output (SPO) compared to the conventional single-flash system and the flash-binary system by up to 148% and 25.6%, respectively, under the same geothermal fluid conditions at the wellhead. Furthermore, it improves the utilization efficiency of the single-flash and combined flash-binary systems by 22 and 7.5 percentage points, respectively. In the economic analysis, it was observed that the additional steam-condensing evaporator is the second-highest capital cost component of the proposed ORC system, accounting for nearly 18% of the total purchased equipment cost. This implies that the ORC system's CAPEX increases by 5.6% compared to the single-flash system. This increase is more than offset by the appreciable improvement in SPO achieved with the ORC system compared to the single-flash system. On the other hand, the proposed ORC system achieves a 19.2% reduction in its CAPEX compared to the flash-binary system.

Since test drilling has not yet been conducted in the study area, an average productivity index value, according to data from commercial geothermal wells, was used as input parameter for the model. However, it was found that variation of this parameter, while it influences the net power output, does not affect the determined optimal operating points.

Future research work is required in this field. In particular, the development of geothermal exploration and research activities are required to better understand the properties of the geothermal fluid. Additionally, the implemented model can provide technical and economic parameters that could serve as a basis for future evaluations, as well as energy planning studies.

CRediT authorship contribution statement

Fernando Montesdeoca-Martínez: Writing – review & editing, Writing – original draft, Visualization, Software, Methodology, Investigation, Formal analysis, Data curation, Conceptualization. **Sergio Velázquez-Medina:** Writing – review & editing, Validation, Supervision, Data curation, Conceptualization. **Stefan Kranz:** Validation, Supervision, Software, Methodology, Data curation, Conceptualization.

Declaration of competing interest

The authors declare that they have no known competing financial interests or personal relationships that could have appeared to influence the work reported in this paper.

Acknowledgements

This research was co-funded with ERDF funds through the INTERREG MAC 2021–2027 programme in the RESMAC project (1/MAC/2/2.2/0011).

F. Montesdeoca-Martínez is a recipient of the pre-doctoral grant (FPU2023/00357) of the Ministry of Science, Innovation and Universities of the Government of Spain. The Erasmus+ Programme (Key Action 131) also supported this research through a grant awarded to F. Montesdeoca-Martínez for a research stay at GFZ Helmholtz Centre for Geosciences.

The authors would like to thank Maren Brehme (ETH Zürich) for helpful comments which substantially improved the quality of the manuscript.

No funding sources had any influence on study design, collection, analysis, or interpretation of data, manuscript preparation, or the decision to submit for publication.

Data availability

Data will be made available on request.

References

[1] World Meteorological Organization. IPCC, 2023: Climate Change 2023: Synthesis Report, https://www.ipcc.ch/report/ar6/syr/downloads/report/IPCC_AR6_SYR_FullVolume.pdf; 2023 [accessed 19 June 2025].

[2] Pombo DV, Martinez-Rico J, Marczinkowski HM. Towards 100% renewable islands in 2040 via generation expansion planning: the case of São Vicente. Cape Verde Appl Energy 2022;315:118869. https://doi.org/10.1016/j.apenergy.2022.118869.

[3] European Commission. Clean energy for EU islands, https://clean-energy-islands.ec.europa.eu/about; 2017 [accessed 19 June 2025].

[4] Psarros GN, Papathanassiou SA. Generation scheduling in island systems with variable renewable energy sources: a literature review. Renew Energy 2023;205:1105–24. https://doi.org/10.1016/j.renene.2023.01.099.

[5] Velázquez Medina S, Carta JA, Portero AU. Performance Sensitivity of a Wind Farm Power Curve Model to Different Signals of the Input Layer of ANNs: Case Studies in the Canary Islands. Complexity 2019;2019:2869149. https://doi.org/10.1155/2019/2869149.

[6] Chen Y, Li X, Chen X, Ding S, Chen Y, Wang W. Identifying time zones of power fluctuations method for photovoltaic power ramp rate optimization. Global Energy Interconnect 2025;8:778–89. https://doi.org/10.1016/j.gloei.2025.05.007.

[7] Meschede H. Increased utilisation of renewable energies through demand response in the water supply sector – a case study. Energy 2019;175:810–7. https://doi.org/10.1016/j.energy.2019.03.137.

[8] Prina MG, Groppi D, Nastasi B, Garcia DA. Bottom-up energy system models applied to sustainable islands. Renew Sustain Energy Rev 2021;152:111625. https://doi.org/10.1016/j.rser.2021.111625.

[9] Aljubran MJ, Horne RN. Techno-economics of geothermal power in the contiguous United States under baseload and flexible operations. Renew Sustain Energy Rev 2025;211:115322. https://doi.org/10.1016/j.rser.2024.115322.

[10] Anderson A, Rezaie B. Geothermal technology: Trends and potential role in a sustainable future. Appl Energy 2019;248:18–34. https://doi.org/10.1016/j.apenergy.2019.04.102.

[11] Matek B. Flexible Opportunities with Geothermal Technology: Barriers and Opportunities. Electr J 2015;28:45–51. https://doi.org/10.1016/j.tej.2015.09.020.

[12] Bhagaloo K, Ali R, Baboolal A, Ward K. Powering the sustainable transition with geothermal energy: a case study on Dominica. Sustainable Energy Technol Assess 2022;51:101910. https://doi.org/10.1016/j.seta.2021.101910.

[13] Kassem MA, Moscariello A. Geothermal energy: a sustainable and cost-effective alternative for clean energy production and climate change mitigation. Sustainable Futures 2025;10:101247. https://doi.org/10.1016/j.sftr.2025.101247.

[14] Fridriksson T, Mateos A, Audinet P, Orucu Y. Greenhouse Gases from Geothermal Power Production. Energy Sector Management Assistance Program (ESMAP) Technical Report 09/16, https://openknowledge.worldbank.org/bitstreams/64df96ca-4476-5d45-b21e-477b87790399/download; 2016 [accessed 19 June 2025].

[15] Graça Gomes J, Xu HJ, Yang Q, Zhao CY. An optimization study on a typical renewable microgrid energy system with energy storage. Energy 2021;234:121210. https://doi.org/10.1016/j.energy.2021.121210.

[16] Spadacini C, Xodo LG, Quaia M. 14 - Geothermal energy exploitation with Organic Rankine Cycle technologies. In: Macchi E, Astolfi M, editors. Organic Rankine Cycle (ORC) Power Systems. Cambridge: Woodhead Publishing; 2017. p. 473–525.

[17] Ricks W, Norbeck J, Jenkins J. The value of in-reservoir energy storage for flexible dispatch of geothermal power. Appl Energy 2022;313:118807. https://doi.org/10.1016/j.apenergy.2022.118807.

[18] Soltani M, Kashkooli FM, Souri M, Rafiei B, Jabarifar M, Gharali K, et al. Environmental, economic, and social impacts of geothermal energy systems. Renew Sustain Energy Rev 2021;140:110750. https://doi.org/10.1016/j.rser.2021.110750.

[19] Liu G, Song J, Zhang W, Cao Q, Yang W, Jiang Z. Environmental footprints of global geothermal power: Bridging micro-level technological and macro-level national assessments. Energ Conver Manage 2026;349:120853. https://doi.org/10.1016/j.enconman.2025.120853.

[20] Sharmin T, Khan NR, Akram MS, Ehsan MM. A State-of-the-Art Review on Geothermal Energy Extraction, utilization, and Improvement strategies: conventional, Hybridized, and Enhanced Geothermal Systems. Int J Thermofluids 2023;18:100323. https://doi.org/10.1016/j.ijft.2023.100323.

[21] Zabek D, Penton J, Reay D. Optimization of waste heat utilization in oil field development employing a transcritical Organic Rankine Cycle (ORC) for electricity generation. Appl Therm Eng 2013;59:363–9. https://doi.org/10.1016/j.applthermaleng.2013.06.001.

[22] Wieland C, Schifflechner C, Dawo F, Astolfi M. The organic Rankine cycle power systems market: recent developments and future perspectives. Appl Therm Eng 2023;224:119980. https://doi.org/10.1016/j.applthermaleng.2023.119980.

[23] He C, Liu C, Gao H, Xie H, Li Y, Wu S, et al. The optimal evaporation temperature and working fluids for subcritical organic Rankine cycle. Energy 2012;38:136–43. https://doi.org/10.1016/j.energy.2011.12.022.

[24] Madhawa Hettiarachchi HD, Golubovic M, Worek WM, Ikegami Y. Optimum design criteria for an Organic Rankine cycle using low-temperature geothermal heat sources. Energy 2007;32:1698–706. https://doi.org/10.1016/j.energy.2007.01.005.

[25] Dai Y, Wang J, Gao L. Parametric optimization and comparative study of organic Rankine cycle (ORC) for low grade waste heat recovery. Energ Conver Manage 2009;50:576–82. https://doi.org/10.1016/j.enconman.2008.10.018.

[26] Papadopoulos AI, Stijepovic M, Linke P. On the systematic design and selection of optimal working fluids for Organic Rankine Cycles. Appl Therm Eng 2010;30:760–9. https://doi.org/10.1016/j.applthermaleng.2009.12.006.

[27] Shengjun Z, Huaixin W, Tao G. Performance comparison and parametric optimization of subcritical Organic Rankine Cycle (ORC) and transcritical power cycle system for low-temperature geothermal power generation. Appl Energy 2011;88:2740–54. https://doi.org/10.1016/j.apenergy.2011.02.034.

[28] Ciucci M. Innovative Technologies in the Development of Geothermal Energy in Europe, https://www.europarl.europa.eu/RegData/etudes/BRIE/2023/754200/IPOL_BRI(2023)754200_EN.pdf; 2023 [accessed 19 June 2025].

[29] Pratama HB, Koike K. Thermodynamic model-based specification of optimal geothermal power generation system for high-temperature liquid-dominated systems using flash and flash-binary cycles. Renew Energy 2024;220:119634. https://doi.org/10.1016/j.renene.2023.119634.

[30] DiPippo R. Geothermal power plants: Evolution and performance assessments. Geothermics 2015;53:291–307. https://doi.org/10.1016/j.geothermics.2014.07.005.

[31] Franco A, Villani M. Optimal design of binary cycle power plants for water-dominated, medium-temperature geothermal fields. Geothermics 2009;38:379–91. https://doi.org/10.1016/j.geothermics.2009.08.001.

[32] Abdolalipouradl M, Mohammadkhani F, Khalilarya S. A comparative analysis of novel combined flash-binary cycles for Sabalan geothermal wells: Thermodynamic and exergoeconomic viewpoints. Energy 2020;209:118235. https://doi.org/10.1016/j.energy.2020.118235.

[33] Hsieh J, Li B, Lee B, Royandi MA, Salsabilla NS. Performance and economic analyses of a geothermal reservoir model coupled with a flash–binary cycle model. Renew Energy 2024;230:120826. https://doi.org/10.1016/j.renene.2024.120826.

[34] Shokati N, Ranjbar F, Yari M. Comparative and parametric study of double flash and single flash/ORC combined cycles based on exergoeconomic criteria. Appl Therm Eng 2015;91:479–95. https://doi.org/10.1016/j.applthermaleng.2015.08.031.

[35] Mokarram NH, Mosaffa AH. Investigation of the thermoeconomic improvement of integrating enhanced geothermal single flash with transcritical organic Rankine cycle. Energ Conver Manage 2020;213:112831. https://doi.org/10.1016/j.enconman.2020.112831.

[36] Schochet DN. Performance of ORMAT Geothermal Binary and combined Steam/Binary Cycle Power Plants with Moderate and High Temperature Resources. Renew Energy 1997;10:379–87.

[37] Franco A, Vieira N, Ponte C, Rangel G. A decade of geothermal commercial production from the Pico Vermelho power plant, São Miguel Island, Azores. In: European Geothermal Congress 2019, Den Haag, The Netherlands; 2019.

[38] Omenda P, Ofwona C, Mangi P. 28 - Kenya: the Most successful Geothermal Development in Africa. In: Dipippo R, Gutiérrez-negrín LCA, Chiasson A, editors. Geothermal Power Generation. Second Edition. Cambridge: Woodhead Publishing; 2024. p. 863–91.

[39] Tranamil-Maripe Y, Cardemil JM, Escobar R, Morata D, Sarmiento-Laurel C. Assessing the Hybridization of an existing Geothermal Plant by Coupling a CSP System for increasing Power Generation. Energies 2022;15(6):1961. https://doi.org/10.3390/en15061961.

[40] Lobos Lillo D, Delgado F, Pritchard ME, Cardona C, Franco L, Pedreros G, et al. Documenting surface deformation at the first geothermal power plant in South America (Cerro Pabellón, Chile) by satellite InSAR time-series. J Volcanol Geoth Res 2023;441:107869. https://doi.org/10.1016/j.jvolgeores.2023.107869.

[41] Vargas-Payera S. Heat in the news: Geothermal energy in Chilean newspaper coverage. Renew Energy 2024;237:121509. https://doi.org/10.1016/j.renene.2024.121509.

[42] Jalilinasrabady S, Itoi R, Uchihori N, Okamura Y. Energy and exergy analysis of geothermal steam binary power generation. GRC Trans 2016;40:49–55.

[43] Lei H, Xie Y, Li J, Hou X. Modeling of two-phase flow of high temperature geothermal production wells in the Yangbajing geothermal field. Tibet Front Earth Sci 2023;11:1019328. https://doi.org/10.3389/feart.2023.1019328.

[44] Cao J, Zheng L, Zheng Z, Peng J, Hu M, Wang Q, et al. Recent progress in organic Rankine cycle targeting utilisation of ultra-low-temperature heat towards carbon neutrality. Appl Therm Eng 2023;231:120903. https://doi.org/10.1016/j.applthermaleng.2023.120903.

[45] Astolfi M. 3 - Technical options for Organic Rankine Cycle systems. In: Macchi E, Astolfi M, editors. Organic Rankine Cycle (ORC) Power Systems. Cambridge: Woodhead Publishing; 2017. p. 67–89.

[46] Astolfi M, Noto La Diega L, Romano MC, Merlo U, Filippini S, Macchi E. Techno-economic optimization of a geothermal ORC with novel "Emeritus" heat rejection units in hot climates. Renew Energy 2020;147:2810–21. https://doi.org/10.1016/j.renene.2019.01.065.

[47] DiPippo R. Geothermal Power Plants: Principles, applications, Case Studies and Environmental Impact. 3rd ed. Kidlington, Oxford, UK: Butterworth-Heinemann (Elsevier); 2012.

[48] F-Chart Software. Engineering Equation Solver (EES), https://fchartsoftware.com/ees/; [accessed 19 June 2025].

[49] Hasan AR, Kabir CS. Modeling two-phase fluid and heat flows in geothermal wells. J Petrol Sci Eng 2010;71:77–86. https://doi.org/10.1016/j.petrol.2010.01.008.

[50] Li X, Song J, Yu G, Liang Y, Tian H, Shu G, et al. Organic Rankine cycle systems for engine waste-heat recovery: heat exchanger design in space-constrained applications. Energ Conver Manage 2019;199:111968. https://doi.org/10.1016/j.enconman.2019.111968.

[51] Browning R. Too cool Robert Browning, Heat transfer Research, Inc., USA, discusses the optimisation of heat exchangers for process cooling in upstream and downstream faciliti. Hydrocarb Eng 2016;21:32–8.

[52] UK Government. Energy Technology Criteria List 2021, https://assets.publishing.service.gov.uk/media/60bfe1f08fa8f57ceec3c85a/etcl-2021-rev-jun-21.pdf; 2021 [accessed 19 June 2025].
[53] KSB. KSB Centrifugal Pump Lexicon - Cooling water pump, https://www.ksb.com/en-global/centrifugal-pump-lexicon/article/cooling-water-pump-1117200; [accessed 19 June 2025].
[54] Blöcher G, Cacace M, Reinsch T, Watanabe N. Evaluation of three exploitation concepts for a deep geothermal system in the north German Basin. Comput Geosci 2015;82:120–9. https://doi.org/10.1016/j.cageo.2015.06.005.
[55] Sanyal SK, Morrow JW, Butler SJ. Geothermal well Productivity: why Hotter is not always Better. GRC Transactions 2007;31:573–9.
[56] Chen NH. An explicit equation for friction factor in pipe. Ind Eng Chem Fundam 1979;18:296–7. https://doi.org/10.1021/i160071a019.
[57] Toth A, Bobok E. Chapter 7 - Flow Through Producing Wells. In: Toth A, Bobok E, editors. Flow and Heat Transfer in Geothermal Systems, Elsevier; 2017, p. 131-160.
[58] Nathenson M. Flashing flow in hot water geothermal wells. J Res US Geol Surv 1974;2:743–51.
[59] Roy JP, Mishra MK, Misra A. Performance analysis of an Organic Rankine Cycle with superheating under different heat source temperature conditions. Appl Energy 2011;88:2995–3004. https://doi.org/10.1016/j.apenergy.2011.02.042.
[60] Turton R, Bailie RC, Whiting WB, Shaeiwit JA. Analysis, Synthesis, and Design of Chemical Processes. 4th ed. New Jersey: Prentice Hall PTR; 2013.
[61] European Union. Document C/2025/03662. Euro exchange rates – 31 July 2025, https://eur-lex.europa.eu/legal-content/EN/TXT/PDF/?uri=OJ:C_202503662; 2025 [accessed 5 December 2025].
[62] Chemical Engineering. The Chemical Engineering Plant Cost Index, https://www.chemengonline.com/pci-home/; [accessed 5 December 2025].
[63] Coskun A, Bolatturk A, Kanoglu M. Thermodynamic and economic analysis and optimization of power cycles for a medium temperature geothermal resource. Energ Conver Manage 2014;78:39–49. https://doi.org/10.1016/j.enconman.2013.10.045.
[64] Fiaschi D, Manfrida G, Rogai E, Talluri L. Exergoeconomic analysis and comparison between ORC and Kalina cycles to exploit low and medium-high temperature heat from two different geothermal sites. Energ Conver Manage 2017;154:503–16. https://doi.org/10.1016/j.enconman.2017.11.034.
[65] Roetzel W, Spang B. C1 Thermal Design of Heat Exchangers. In: VDI e.V., editors. VDI Heat Atlas. VDI-Buch, Berlin, Heidelberg: Springer; 2010.
[66] Cartaxo SJM, Fernandes FAN. Counterflow logarithmic mean temperature difference is actually the upper bound: a demonstration. Appl Therm Eng 2011;31:1172–5. https://doi.org/10.1016/j.applthermaleng.2010.12.015.
[67] Lecompte S, Van den Broek M, De Paepe M. Optimal selection and sizing of heat exchangers for organic Rankine cycles (ORC) based on thermo-economics. In: 15th International Heat Transfer Conference, IHTC-15, Kyoto, Japan; 2014.
[68] Ali S, Faraj J, Khaled M. A correlation for U-value for laminar and turbulent flows in concentric tube heat exchangers. Int J Thermofluids 2024;23:100797. https://doi.org/10.1016/j.ijft.2024.100797.
[69] F-Chart Software. EES Manual, https://www.fchart.com/assets/downloads/ees_manual.pdf; [accessed 5 December 2025].
[70] Brent RP. Algorithms for Minimization without Derivatives. New Jersey: Prentice-Hall; 1973.
[71] Bahrami M, Pourfayaz F, Kasaeian A. Low global warming potential (GWP) working fluids (WFs) for Organic Rankine Cycle (ORC) applications. Energy Rep 2022;8:2976–88. https://doi.org/10.1016/j.egyr.2022.01.222.
[72] Braimakis K, Karellas S. Exergetic optimization of double stage Organic Rankine Cycle (ORC). Energy 2018;149:296–313. https://doi.org/10.1016/j.energy.2018.02.044.
[73] Pambudi NA, Itoi R, Jalilinasrabady S, Jaelani K. Performance improvement of a single-flash geothermal power plant in Dieng, Indonesia, upon conversion to a double-flash system using thermodynamic analysis. Renew Energy 2015;80:424–31. https://doi.org/10.1016/j.renene.2015.02.025.
[74] National Statistics Institute (Spain). Continuous population statistics, https://www.ine.es/; 2025 [accessed 19 June 2025].
[75] Tourism of Tenerife. Tourist situation of Tenerife 2024, https://www.webtenerife.com/-/media/files/investigacion/situacion-turistica/informes-de-situacin-turstica-de-tenerife/relateddocuments/2024/balance-de-situacin-turstica-de-tenerife-2024.pdf; 2025 [accessed 19 June 2025].
[76] Canary Islands Government. Annual energy report for The Canary Islands 2023, https://www.gobiernodecanarias.org/energia/descargas/SDE/Portal/Publicaciones/AnuarioEnergeticodeCanarias-2023.pdf; 2025 [accessed 19 June 2025].
[77] Canary Islands Government. Canary Islands Dispatchable Generation Strategy (v1 edition), https://www.gobiernodecanarias.org/energia/descargas/oecan/D4_Estrategia_Generaci%C3%B3n_Gestionable.pdf; 2022 [accessed 19 June 2025].
[78] Canary Islands Government. Geothermal Strategy in the Canary Islands, https://www.gobiernodecanarias.org/energia/descargas/oecan/D5_Estrategia_Geotermia_Canarias.pdf; 2020 [accessed 19 June 2025].
[79] Geological and Mining Institute of Spain (IGME). Geothermal exploration in the central area of the island of Tenerife, https://info.igme.es/SidPDF/172000/910/172910_0000003.pdf; 1993 [accessed 19 June 2025].
[80] Government of Spain. GEOTHERCAN Project, https://datos.gob.es/es/solicitud-de-datos/proyecto-geothercan-referencia-ipt-2011-1186-920000; [accessed 19 June 2025].
[81] Institute for Technology and Renewable Energies (ITER), https://www.iter.es/; [accessed 19 June 2025].
[82] Petratherm Limited, https://www.petratherm.com.au/; [accessed 19 June 2025].
[83] Volcanology Institute of the Canaries (INVOLCAN), https://involcan.org/; [accessed 19 June 2025].
[84] Petratherm Limited. Petratherm 2012 Annual Report. Clean Energy for Future Generations, https://www.annualreports.com/HostedData/AnnualReportArchive/p/ASX_PTR_2012.pdf; 2012 [accessed 19 June 2025].
[85] Trainor-Guitton WJ, Hoversten GM, Nordquist G, Intani RG. Value of MT inversions for geothermal exploration: Accounting for multiple interpretations of field data & determining new drilling locations. Geothermics 2017;66:13–22. https://doi.org/10.1016/j.geothermics.2016.11.009.
[86] Hidalgo R. High enthalpy projects in the Canary Islands. In Technical Seminar: Low enthalpy geothermal energy: a look into the future, https://arquitectosgrancanaria.es/medios/documents/eventos/121018_programa.pdf; 2012 [accessed 19 June 2025].
[87] Pérez N. Tenerife Geothermal Power Project: an energy challenge for the sustainability development of the island, https://rac-ciencias.org/wp/wp-content/uploads/2019/05/ZZnemesioperz.pdf; [accessed 19 June 2025].
[88] Rodríguez F, Pérez NM, Melián GV, Padrón E, Hernández PA, Asensio-Ramos M, et al. Exploration of deep-seated geothermal reservoirs in the Canary Islands by means of soil CO_2 degassing surveys. Renew Energy 2021;164:1017–28. https://doi.org/10.1016/j.renene.2020.09.065.
[89] Chen Y, Dai B, Ren W, Niu H, Chen Z. A comprehensive review of energy security in islanded regions: challenges, strategies, and sustainable development pathways. Renew Sustain Energy Rev 2025;220:115879. https://doi.org/10.1016/j.rser.2025.115879.
[90] Eberle A, Heath G, Carpenter Petri A, Nicholson S. Systematic Review of Life Cycle Greenhouse Gas Emissions from Geothermal Electricity, https://www.nrel.gov/docs/fy17osti/68474.pdf; 2017 [accessed 5 December 2025].
[91] Astolfi M, Martelli E, Pierobon L. 7 - Thermodynamic and technoeconomic optimization of Organic Rankine Cycle systems. In: Macchi E, Astolfi M, editors. Organic Rankine Cycle (ORC) Power Systems. Cambridge: Woodhead Publishing; 2017. p. 173–249.
[92] Li W, Ling X. A novel analysis framework for the organic Rankine cycle waste heat recovery system: from the viewpoint of turbine design. Case Stud Therm Eng 2022;32:101830. https://doi.org/10.1016/j.csite.2022.101830.
[93] Nazari N, Heidarnejad P, Porkhial S. Multi-objective optimization of a combined steam-organic Rankine cycle based on exergy and exergo-economic analysis for waste heat recovery application. Energ Conver Manage 2016;127:366–79. https://doi.org/10.1016/j.enconman.2016.09.022.
[94] Li P, Shu C, Li J, Wang Y, Chen Y, Ren X, et al. Thermodynamic Investigation and Economic Evaluation of a High-Temperature Triple Organic Rankine Cycle System. Energies 2023;16(23):7818. https://doi.org/10.3390/en16237818.
[95] Roetzel W, Spang B. C3 Typical Values of Overall Heat Transfer Coefficients. In: VDI e.V., editors. VDI Heat Atlas. VDI-Buch, Berlin, Heidelberg: Springer; 2010.
[96] Åkesjö A, Gourdon M, Jongsma A, Sasic SM. Enhancing industrial vertical falling film evaporation through modification of heat transfer surfaces – an experimental study. Chem Eng Process - Process Intesif 2023;191:109456. https://doi.org/10.1016/j.cep.2023.109456.
[97] Dimian A, Bildea CS. Appendix B: Heat-Exchanger design. In: Dimian A, Bildea CS, editors. Chemical Process Design: Computer-Aided Case Studies. Weinheim: Wiley-VCH; 2008. p. 474–82.